Journal of Building Engineering 127 (2026) 116371

Contents lists available at ScienceDirect

Journal of Building Engineering

journal homepage: www.elsevier.com/locate/jobe

Utilisation of biomass and waste-derived ashes in the extrusion of fired clay bricks: mechanical properties, microstructure and leaching behaviour

Lea Žibret, Majda Pavlin, Vilma Ducman *

Laboratory for Cements, Mortars and Ceramics, The Department of Materials, Slovenian National Building and Civil Engineering Institute (ZAG), Dimičeva ulica 12, 1000, Ljubljana, Slovenia

ARTICLE INFO

Keywords:
Biomass and waste derived ashes
Clay
Extruded fired bricks
Ceramic-technological tests
Microstructure
Leaching

ABSTRACT

With the trend towards renewable alternatives to fossil fuel sources, further uses of biomass and waste ash instead of landfilling are being explored. This study investigates the potential of fly and bottom ashes from burning wood (alone or with coal), as well as coal-co-combustion of municipal solid waste, sewage sludge, and paper sludge, for use in extruded fired bricks fired at 950 °C. The influence of ash content (0 to 15 wt% ash) and ash type (10 wt% ash) on the physical, mechanical, and microstructural properties of the fired bricks was studied. The compressive strength of the reference sample without ash was 72.6 MPa and decreased gradually with an increasing ash content. Open porosity ranged from 28% (reference, no ash) to 43% (15 wt% ash), and water absorption from 12% to 28%, reflecting the pore-forming role of the added ashes. All samples had a compressive strength above the 10 MPa limit specified in EN 772-1, except for bricks with 5 wt % paper sludge bottom ash (B4, W-PS BA). The leaching concentrations indicate that heavy metals were effectively immobilised within the ceramic structure of the fired bricks, relative to inert and non-hazardous waste limit values under EN 12457-2 test conditions. These results suggest that 5% substitution of primary raw materials with ashes may contribute to the production of bricks with reduced environmental impact and improved resource efficiency. The study provides a basis for further formulation of extruded bricks with biomass and waste-derived ashes.

1. Introduction

The growing world population leads to increasing amounts of unavoidable biomass and municipal solid waste (MSW). Their combustion and co–combustion with coal in thermal and power plants enables a gradual and simultaneous reduction in coal consumption and an increase in the utilization of wastes [1]. The by-product of such a process is ash, which can be, similar to coal combustion ash [2], used in various construction materials, avoiding their landfilling and promoting the circular economy and zero-waste approach [3]. Significant quantities of such ash can be used to replace clay in the brick industry [4–9].

Reusing such ashes usually requires a specific pretreatment for the removal of contaminants [10–12]. Previous studies have shown that the leaching of heavy metals from fired bricks is significantly lower than from unfired bricks [13,14]. Furthermore, thermal

* Corresponding author.
E-mail address: vilma.ducman@zag.si (V. Ducman).

https://doi.org/10.1016/j.jobe.2026.116371
Received 10 February 2026; Received in revised form 10 May 2026; Accepted 21 May 2026
Available online 22 May 2026

treatments efficiently remove dioxins from ash, making it one of the most promising methods to ensure the safe use of ash [13]. The incorporation of ash into fired bricks ensures a safe handling of ash through its direct use, which can avoid the cost of ash treatment and reduce the cost of brick production [13]. Non-plastic additives, such as ashes, disrupt clay alignment during extrusion and reduce water retention, resulting in stiffer, less deformable material with reduced plasticity and drying shrinkage [15]. However, there is a scientific gap in studies evaluating the influence of ash addition on the properties of extruded mass for clay brick production. Several researchers have investigated the replacement of clay with MSW ash [13,16], sewage sludge (SS) ash [17,18], biomass ash [19–21] and paper sludge (PS) ash [22] in fired clay bricks with up to 50 wt% of ashes. The firing temperature of the bricks was between 950 °C [13] and 1050 °C [16]. All noted studies feature bricks produced by pressing into moulds and concluded that an ash content of up to 20 wt% results in acceptable bricks. However, the industrial scale production of bricks is performed via vacuum extrusion, which results in a denser and less porous structure [23–25], which might allow higher amounts of incorporated ash. In order to mimic the conditions of an industrial scale production, brick samples for ceramic technology tests can be produced using laboratory extrusion equipment [26–29].

In fired bricks, biomass ash acts as a pore-forming additive that increases the porosity of the bricks and can weaken the mechanical properties of the final products [19]. Similar to biomass ash, admixed MSWI ash was reported to alter the microstructure of bricks, resulting in lower compressive strength and density as well as increased porosity and water absorption [30]. On the other hand, clay discs with MSWI ash in the study of Kirkelund et al. showed a low porosity and water absorption. The addition of SS to the fired bricks resulted in an apparent density and open porosity within the expected range of 1610-2120 kg/m^3 and 19-39 vol% [18,31]. The mechanical properties and water absorption, porosity and durability of extruded clay bricks strongly depend on the type of clay, and microstructure of the matrix [25,32].

European Landfill directive [33] defines the permissible limits for toxic elements including Cr, Ni, Cu, Zn, As, Se, Mo, Cd, Sb, Ba, Hg and Pb. The leaching properties, along with the mineralogical and chemical composition of a material, can also provide indirect information about the immobilisation potential of heavy metals [34,35]. The type of fuel used in thermal power plants and boilers influences the mineralogical, chemical, and physical properties of the produced ash [36]. Therefore, replacing parts of the natural clay brick raw mix by biomass ashes affects the mechanical and environmental properties of the fired clay bricks. Due to the global trend of accelerated transition to the use of renewable energy sources, additional studies on the influence of biomass ashes (either pure or co-fired with coal) on the mechanical and environmental properties of the fired clay bricks with such ashes are urgently needed to ensure safe ash management and prevent their landfilling. Some studies on the application of biomass ashes in fired bricks are available, but the properties of ashes and bricks cannot be compared directly due to variation in mineralogical and chemical composition of clays as well as ashes, therefore experimental confirmation of usability of specific ash with specific clay is needed. Therefore in the present study ashes from four manufacturers are evaluated for use in extruded bricks fired at 950 °C, including wood (W) biomass ash (pure or co-fired with coal), ash from the co-firing of SS and MSW, and ash from the co-firing of coal, W biomass and PS. The study presents the results of chemical and mineralogical characterisation of ashes and comprehensive technological tests of bricks, performed using consistent analytical protocols, which allow direct evaluation of the ashes in brick production. The key advances are: (i) the simultaneous and direct comparison of fly ash and bottom ash from the same source under identical processing conditions; (ii) the systematic evaluation of eight ashes spanning chemically distinct categories (Ca-rich wood ash, high-salt MSW-SS FA, and mixed-fuel ashes); and (iii) their evaluation in a vacuum extrusion process replicating industrial practice. This multi-dimensional comparative framework, conducted under consistent analytical protocols, provides a unified basis not available from previous single- or dual-ash studies. The variation of properties is discussed from two points of view: the amount of ash added and the microstructural characteristics. The potential impact of such products on the environment is evaluated on the basis of the leaching

Table 1
Brick raw mixtures (% by dry mass) prepared by clay (C) and ashes (F1 – F4 and B1 – B4) and fraction >1 mm (wt%). Abbreviations: BC = brown coal; W = wood; MSW = municipal solid waste; SS = sewage sludge; PS = paper sludge.

Sample designation	Fuel type for ash	Incineration plant	F1	B1	F2	B2	F3	B3	F4	B4	C
A-0	-		-	-	-	-	-	-	-	-	100
A-2	BC-W	1	5	-	-	-	-	-	-	-	95
A-1	BC-W	1	10	-	-	-	-	-	-	-	90
A-3	BC-W	1	15	-	-	-	-	-	-	-	85
A-4	BC-W	1	-	5	-	-	-	-	-	-	95
A-5	BC-W	1	-	10	-	-	-	-	-	-	90
A-6	BC-W	1	-	15	-	-	-	-	-	-	85
A-7	MSW-SS	2	-	-	-	5	-	-	-	-	95
A-8	MSW-SS	2	-	-	-	10	-	-	-	-	90
A-9	W	3	-	-	-	-	-	5	-	-	95
A-10	W	3	-	-	-	-	-	10	-	-	90
A-11	W	3	-	-	-	-	5	-	-	-	95
A-12	W	3	-	-	-	-	10	-	-	-	90
A-13	MSW-SS	2	-	-	5	-	-	-	-	-	95
A-14	MSW-SS	2	-	-	10	-	-	-	-	-	90
A-15	W-PS	4	-	-	-	-	-	-	-	5	95
A-17	BC-W-PS	4	-	-	-	-	-	-	5	-	95
A-18	BC-W-PS	4	-	-	-	-	-	-	10	-	90
Fraction > 1 mm (wt%)			2.9	47.2	0.3	20.9	1.4	7.6	1.8	33.9	

properties in water. The main research questions are: (i) How do fly ash versus bottom ash from the same combustion source affect porosity, crack development, and compressive strength of bricks fired at 950 °C? (ii) What ash types and substitution dosages can be incorporated while still achieving the EN 772-1 compressive strength standard? (iii) Are the resulting fired bricks classifiable as inert or non-hazardous waste under the European Landfill Directive, and which elements pose the greatest leaching risk?

2. Materials and methods

The basic raw material in this study was a mixture of marl (50 wt%), clay (48 wt%) and coal powder (2 wt%) taken from regular production of clay bricks. Clay and marl came from a quarry in western Slovenia. We have added a short paragraph in the Materials section. The clay-marl mix used exhibits a Pfefferkorn plasticity value of 1.48, which is relatively high compared to average European brick clays (typical range 1.0–1.6), and a carbonate content of approximately 4 wt% CaO (Table 2), which is within the normal range. Eight ashes were used, originating from 4 incinerators burning different materials, including fly ash (FA) and bottom ash (BA) from each site (Table 1): (i) brown coal (BC), wood (W) (F1, B1); (ii) MSW and SS (F2, B2); (iii) wood (W) (F3, B3); (iiii) brown coal (BC), wood (W), paper sludge (PS) (F4) and paper sludge (PS) (B4). B4 is a mixture of FA (20%) and BA (80%). The ashes were sieved using a sieve with 1 mm diameter openings. The fractions <1 mm were used in brick mixtures, while particles >1 mm were discarded. No additional grinding was applied. The weight percentages of the fraction >1 mm, determined by dry sieving [37], are given in Table 1. These data may be beneficial for potential future evaluation of industrial applicability and processing-related costs.

The particle size distribution (PSD) of ashes and clay was measured by laser diffraction granulometry using a Sync + FlowSync laser particle size analyzer (Microtrack MRB) in wet dispersion measurement mode. The dispersion medium for the ash was isopropanol, while the clay was analysed in distilled water with the addition of a dispersant (5 % Sodium pyrophosphate solution). The ash was sieved to a particle size of less than 0.25 mm for this measurement.

The chemical composition of the raw materials was determined with an ARL PERFORM'X sequential X-ray fluorescence (XRF) spectrometer (Thermo Fisher Scientific Inc., Ecublens, Switzerland) using the UniQuant 5 software (Thermo Fisher Scientific Inc., Walthem, MA, USA). The samples were previously ignited at 950 °C for 2 h and then mixed with Fluxana (Li tetraborate and Li metaborate in a 1:1 mass ratio) at a ratio of 1:10 and melted into discs. LiBr(l) (50 mL H2O and 7.5 g LiBr(s) from Sigma Aldrich) was added to the mixture. Due to the high sodium and chlorine content (halite) of sample F2, XRF was performed on the non-ignited sample (pressed pellets with the ratio sample: celuluse 5:1).

The XRD examination of raw materials and bricks was carried out using a PANalytical Empyrean X-ray diffractometer with CuKα radiation (wavelength CuKα1 1.54 Å). The samples were ground to a grain size of less than 63 μm and manually back–loaded into a cylindrical sample holder (diameter 27 mm). Each sample was measured from $2\theta = 4°$ to 70° with an increment of 0.0130° as it was rotated. The X–ray tube was operated at 45 kV and 40 mA. Phase determination was performed using PANalytical X'Pert High Score Plus Diffraction software v. 4.8. using the structures for the phases from the ICDD PDF 4 + 2016 RDB powder diffraction files. The amorphous content was determined using the external standard NIST 676a.

Approximately 20 kg of each mixture were shaped in three main shapes using a laboratory vacuum extruder (Karl Händle & Söhne Mühlacker, type PZVMga): cylinders (mould diameter = 56.3 mm; extruded length = 55 mm), prisms (mould dimensions: 54.3 × 27.7 mm^2; extruded length = 150 mm) and tiles (mould dimensions: 57.2 × 9.3 mm^2; extruded length = 150 mm). Extruded tiles were cut

Table 2
Chemical composition of raw materials (except F2, all ignited at 950 °C) measured by XRF. The LOI for ignited samples and the main percentiles of the PSD are also given. Abbreviations: F1-F4 = FA; B1-B4 = BA; C = brick clay-marl mix. The margin of error is considered to be ±0.1 wt%.

	F1	B1	F2	B2	F3	B3	F4	B4	C
Na_2O (wt%)	0.3	0.5	30.2	1.9	0.6	0.4	0.9	0.7	0.8
MgO (wt%)	8.2	10.4	1.8	3.8	3.7	6.2	6.2	2.2	1.7
Al_2O_3 (wt%)	10.7	6.5	9.0	16.6	6.6	3.0	11.2	10.9	15.6
SiO_2 (wt%)	28.2	30.1	9.0	26.4	18.6	5.3	23.1	14.2	59.0
P_2O_5 (wt%)	0.6	1.0	1.0	2.6	2.2	3.1	0.3	0.3	0.1
SO_3 (wt%)	1.7	0.1	3.1	1.0	1.0	0.3	1.7	0.3	0.2
Cl (wt%)	0.0	0.0	22.4	0.4	0.1	0.0	0.2	0.1	0.0
K_2O (wt%)	2.2	3.2	3.8	0.5	5.6	8.7	1.1	0.3	2.2
CaO (wt%)	20.0	31.0	15.0	30.7	28.3	47.0	33.9	55.4	4.1
TiO_2 (wt%)	0.5	0.3	1.1	2.0	0.4	0.1	0.8	0.2	0.7
Cr_2O_3 (wt%)	0.0	0.0	0.1	0.1	0.0	0.0	0.0	0.0	0.0
MnO (wt%)	0.3	0.0	0.1	0.2	0.4	0.0	0.1	0.0	0.2
Fe_2O_3 (wt%)	10.6	0.3	1.4	3.4	1.7	1.0	8.4	0.4	6.0
Co_3O_4 (wt%)	0.0	3.6	0.0	0.0	0.0	0.7	0.0	0.0	0.0
CuO (wt%)	0.0	0.0	0.1	0.3	0.0	0.0	0.0	0.1	0.0
ZnO (wt%)	0.0	0.0	1.2	0.8	0.0	0.0	0.2	0.0	0.0
As_2O_3 (wt%)	0.1	0.1	0.4	0.1	0.1	0.1	0.1	0.1	0.1
SrO (wt%)	0.1	0.0	0.0	0.0	0.1	0.1	0.1	0.1	0.0
ZrO_2 (wt%)	0.0	0.0	0.0	0.1	0.0	0.0	0.0	0.0	0.0
BaO (wt%)	0.2	0.1	0.1	0.2	0.1	0.3	0.2	0.0	0.0
Other (wt%)	0.1	0.0	0.2	0.2	0.0	0.1	0.1	0.0	0.0
LOI 950 °C (wt%)	16.3	12.9	*	8.9	30.6	23.6	11.4	14.7	9.0

into smaller samples (57.2 mm × 9.3 mm x 25 mm) for firing in a gradient furnace. Samples were prepared at a constant extrusion speed and a constant pressure of approximately 0.9 kg/cm^2. The brick mixtures were prepared according to (Table 1) with clay and up to 15 wt% ashes. Namely, 5, 10 and 15 wt% replacements were tested for F1 and B1 ashes, but due to the difficulty of shaping at 15 wt % ash (extruded shapes were cracked at the edges), 5 and 10 wt% replacements were tested for other ashes (except B4, where only 5 wt % ash was possible as a replacement for clay due to cracking during extrusion). An extruded specimen was considered unacceptable if visible macroscopic cracks at the edges exceeded approximately 10 mm in length, or if multiple cracks were present across the cross-section, making the specimen geometrically unsuitable for standard ceramic-technological testing. The plasticity was determined using the Pfefferkorn method which is based on impact deformation and determines the amount of water required to achieve a contraction of 30% of the initial height of a test specimen under the action of a standard mass [38,39]. The specimens for Pfefferkorn method were cylindrical, with a height of 40 mm and a diameter of 30 mm. The distance between the hammer and the sample was 150 mm. The extruded samples were gradually dried: 3 days at room temperature and covered with a plastic bag, 3-5 days at room temperature uncovered, 6-8 h at 45 °C and 16-20 h at 110 °C, in an air stream. For each mixture, nine specimens of the smallest tiles

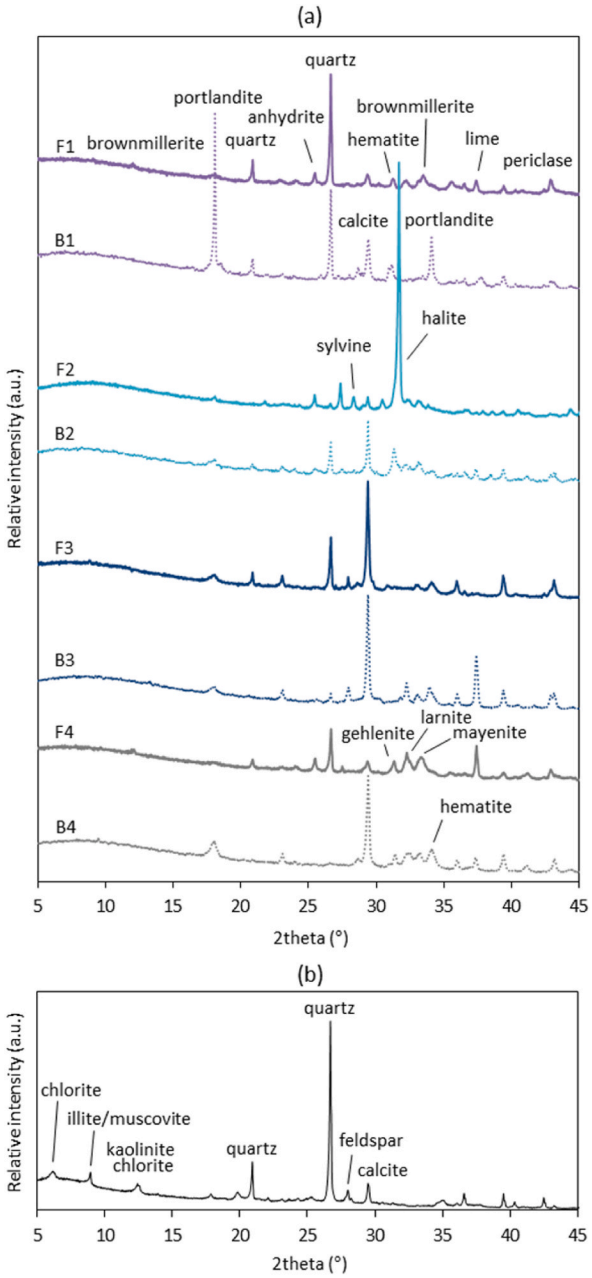

Fig. 1. XRD patterns of (a) ash (F1 - F4 and B1 - B4) and powdered clay (C). The characteristic reflections of identified major phases are highlighted.

were fired in a gradient kiln at a heating rate of 150 °C/h with a holding time of 20 min. Each tile was fired at an individual temperature using nine heaters, with temperatures ranging from approximately 750 °C or 850 °C to around 1140 °C. For the comparison of shrinkage and water absorption at 950 °C, the closest data point (heater) below 950 °C was selected. The water absorption of the samples fired in the gradient furnace was determined after gradual immersion in distilled water (immersion of one quarter of the length per hour for 4 h) and subsequent boiling for 2 h. Cylinders, prisms and tiles were fired in a chamber kiln at 950 °C, with a heating rate of 150 °C/h and a holding time of 2 h.

The compressive strength was measured on fired cylinders using a ToniNORM (ToniTechnik, Berlin, Germany) at a force rate of 0.5 kN/s, while the bending strength was measured on fired prisms using a Gabbrielli tile strength tester. The compressive strength was measured on 5 specimens and the bending strength on seven specimens. Drying and firing shrinkage was calculated from the difference in the length of the 50 mm lines impressed on the fresh prisms, before/after firing (7 samples, 2 measurements for each; the reported result is an average of 14 values). The density of the fired prisms was calculated from the measured dimensions and mass. The water absorption was determined after the prisms had been boiled in water for 2 h (the cooled samples were weighed) [40].

The pore distribution of the manufactured bricks was measured using Mercury intrusion porosimetry (MIP). Small representative fragments (one representative fragment per brick mixture) were dried in an oven (Binder) at 105 °C under a laboratory atmosphere to a constant mass and analysed with a Micromeritics® Autopore IV 9500 (Micromeritics, Norcross, GA, USA).

Bricks were cut in two directions (parallel and perpendicular to the extrusion direction), cast in epoxy resin, dry polished and coated with a carbon layer of approximately 15 nm thickness. Samples were examined by scanning electron microscopy (SEM) and energy dispersive x-ray spectroscopy (EDXS) using a JEOL IT500 LV SEM equipped with an Ultim Max detector (Oxford Instruments) operated in high vacuum mode with an accelerating voltage of 15 kV. EDXS was evaluated using the Aztec 5.0 SP1 software (Oxford Instruments Nanotechnology Tools Ltd). The pore diameters and crack widths were measured using the 'ruler' tool of the SEM software in two cross sections; parallel (P) and perpendicular (V) to the extrusion direction. To minimise the influence of the measurement of apparent pore diameters and crack widths in 2D cross-sections, a large number of measurements was taken and statistically evaluated (histograms, average values). Pore diameters and crack widths were measured systematically over an area of approximately 1 cm × 1.5 cm on the polished cross-section (the entire area was examined), for one representative brick specimen per mixture.

The leaching tests were carried out in accordance with the standard EN 12457-2:2002 [41]. Brick fragments were crushed to below 4 mm. The mixture was agitated for 24 h with the liquid to solid (L:S) ratio 10, after which the suspension was filtered through a 0.45 μm membrane filter prior to ICP-MS analysis, in accordance with standard procedure EN 12457-2. The concentrations of heavy metals were analysed by inductively coupled plasma-mass spectrometer (ICP-MS; Agilent 7900 ORS). Prior to analysis, all samples were acidified, and each measurement was performed twice to ensure reproducibility, with the average values used for data analysis.

3. Results and discussion

3.1. Characterization of the raw materials

Table 2 presents the chemical composition and particle size distribution (PSD) of the raw materials used, while Fig. 1 illustrates their mineralogical composition. The images of the raw materials are provided in Supplement 1 and are partly sourced from Ref. [42]. The main crystal phases were quartz, calcite, illite/muscovite, kaolinite, feldspars and chlorite. FA were coarser than BA, with the exception of B4, which is a mixture of FA and BA. Ashes from the co-combustion of BC and W (F1, B1) had the highest SiO_2 content, with similar values for FA and BA, related to quartz. The quartz phase transformation at 573 °C may generate local stresses. The FA (F1) had the highest Fe_2O_3 content of all ashes, mainly related to hematite (there was also an indication of brownmillerite), while the BA had the highest MgO content, mainly due to periclase, which can undergo a hydration reaction generating micro-stresses. The composition of the ashes from MSW and SS incineration (F2, B2) differed significantly for FA and BA. F2 had a very high Na_2O and Cl content, related to halite, while B2 had the highest Al_2O_3 content, related to calcium aluminate phases (gehlenite, mayenite). Ashes from the incineration of W, PS and the co-combustion of BC, W and PS had the highest CaO content, related to calcite and lime, which cause delayed expansive reactions. For both incinerators, BA (B3, B4) contained about 30 wt% more CaO than FA (F3, F4). Based on PSD, FA were coarser than BA, except for B4, which is a mixture of FA and BA (Table 3).

3.2. Physical and mechanical properties of bricks with ashes

Samples were first fired in a gradient kiln at temperatures up to approximately 1130 °C, combined with a water absorption test, to demonstrate the effect of firing temperature on shrinkage and water absorption (Fig. 2). Replacing the clay-marl mixture with ash resulted in reduced shrinkage and significantly increased the open porosity. For example, the firing shrinkage and water absorption of

Table 3
The main percentiles of the particle size distribution for raw materials, measured by laser diffraction (fraction <250 μm). Abbreviations: F1-F4 = FA; B1-B4 = BA; C = brick clay-marl mix.

	F1	B1	F2	B2	F3	B3	F4	B4	C
PSD d_{90} (μm)	207.1	235.5	88.1	197.4	228.1	239.1	234.8	228.9	204.1
PSD d_{50} (μm)	28.4	44.3	18.0	31.2	31.9	27.5	32.5	11.9	8.4
PSD d_{10} (μm)	5.0	4.7	5.1	4.4	8.8	5.2	4.6	1.8	1.2

the pure clay-marl sample (sample A-0) at around 950 °C were 1.0% and 13.0%, whereas the firing shrinkage and water absorption of the sample with clay-marl mixture and 15 wt% ash (BC, W; sample A-3) at around 950 °C were 1.2% and 26.8%. At approximately 950 °C, water absorption ranged from 13.0% (A-0) to 26.8% (A-3), and firing shrinkage from 0.3% (A-14) to 1.9% (A-11). In general, a progressive closure of open porosity due to vitrification occurred at temperatures above approximately 1050 °C. Bricks with 10 wt%

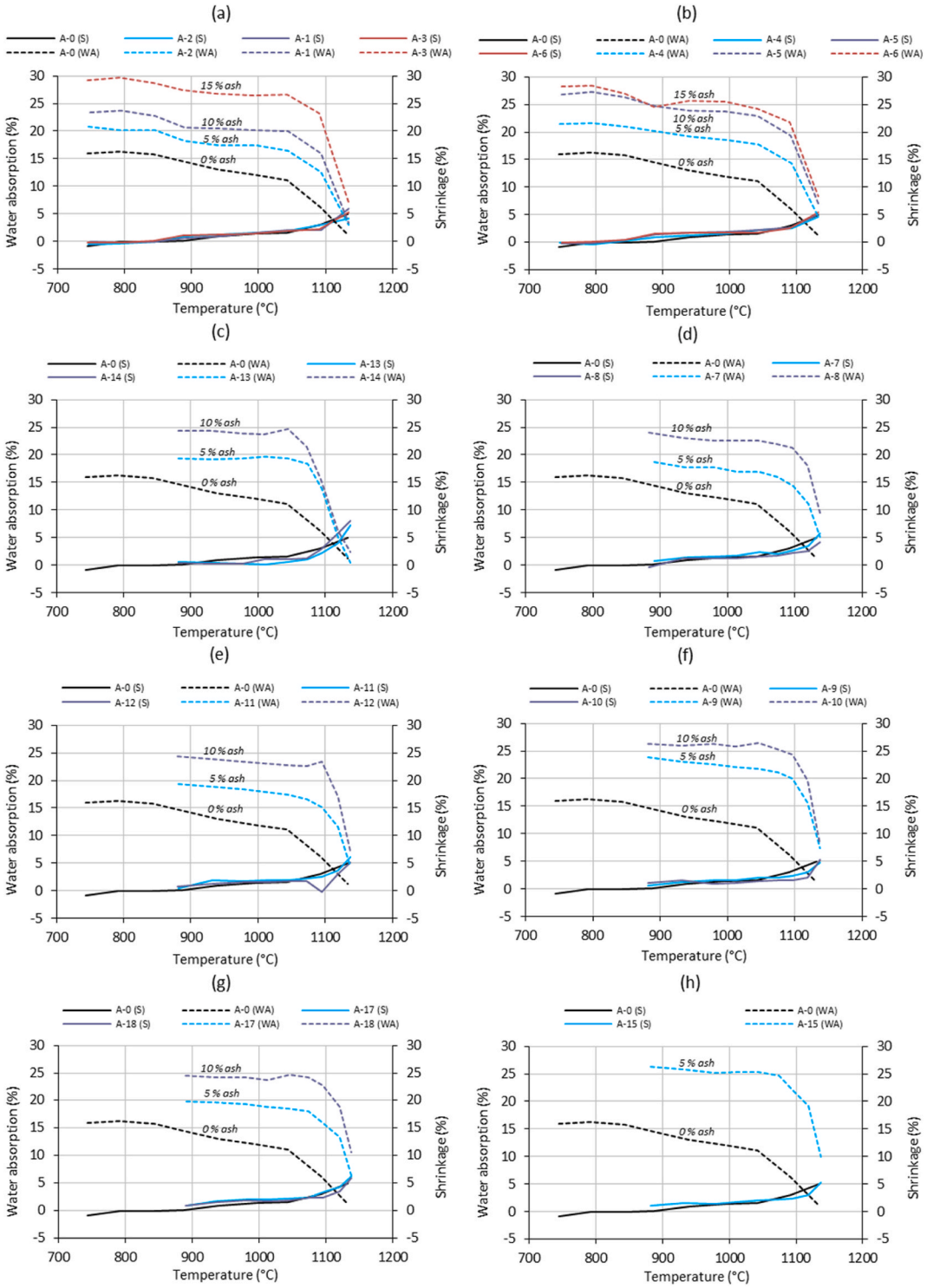

Fig. 2. The effect of firing temperature on the shrinkage and water absorption of brick samples with different ashes (S denotes shrinkage and WA water absorption): (a) F1; (b) B1; (c) F2); (d) B2; (e) F3; (f) B3; (g) F4; (h) B4.

MSW-SS FA (A-14) reached the highest water absorption at approximately 1050 °C, showing no deviation in the shrinkage curve (Fig. 2c). On the other hand, bricks with 10 wt% WFA (A-12) showed an increase in open porosity at around 1100 °C, accompanied by expansion (Fig. 2e). The sample contained ash with lime and very high calcite content, which during firing transformed to lime. At the highest porosity level, water accessed the pores and reacted with lime, resulting in expansion. The study aimed to determine the optimal ash-clay mixture for pilot production at a Slovenian brick factory. For the ceramic-technological tests, a firing temperature of 950 °C was used, as this is the temperature applied in the company's regular brick production. The clay-marl mix used exhibits a Pfefferkorn plasticity value of 1.48, which is relatively high compared to average European brick clays (typical range 1.0–1.6) and indicate highly plastic material sensitive to moisture changes. The mix contained approximately 4 wt% CaO (Table 2), which is within the normal range for Central Europe [43,44].

The mixture properties during shaping, drying, and firing at 950 °C are shown in Table 4. Higher ash content required increased mix moisture. This is related to the greater water demand of the mixture due to the incorporation of non-plastic ashes [45,46]. Mixtures requiring very high moisture to achieve workability (e.g. W-BC FA, A-3 at 33.92%) experienced enhanced clay alignment during extrusion (Supplement 4). This elevated alignment resulted in higher drying shrinkage, amplified crack widths upon thermal treatment, and consequently reduced compressive strength. The exceptions were mixes with F2 (MSW-SS FA) and B3 (W BA) ashes, where a 10 wt% ash mix had a lower water demand than a 5 wt% ash mix, and mixes with F4 (BC-W FA), where 5 and 10 wt% ash had similar water requirements. MSW-SS FA contains significant amount of halite which decreases plastic limit and increases the flowability of illite clay, which can explain the specific water demand behaviour [47]. On the other hand, W BA (F4) and BC-W FA (F4) contained the larger amounts of large particles, which probably affected water demand. 15 wt% ash required a moisture of around 33% to achieve high plasticity, which made the raw mix difficult to shape and resulted in cracks at the edges of extruded specimens. Consequently, an ash content of 15 wt% was considered to be too high for the investigated type of clay. In industrial practice, the moisture of the extrusion mix is typically controlled within narrow limits (often 20–27 wt%) to maintain die pressure and throughput stability; exceeding these limits would require adaptation of the extrusion line parameters. We therefore recommend that industrial trials be limited to 5–10 wt% ash substitution as a conservative starting point.

Drying shrinkage decreased with an increasing ash content, which confirmed the findings of previous studies [48]. The exception was the mix with 15 wt% ash F1, where the drying shrinkage increased, probably due to the highest moisture of mix A-3, which was not compensated by the ash. However, mix A-6 showed similar moisture to A-3 but lower drying shrinkage. This is probably related to the presence of larger particles. Drying shrinkage depends on the mean particle size [49], namely shrinkage was smaller in BA which contains coarser particles. Conversely, firing shrinkage was lower in FAs, most likely due to the higher carbonate content in BA. The increased firing shrinkage of mixtures with ash F4 may be attributed to the formation of metastable phases [50]. The samples with ash F2 (MSW-SS FA) disintegrated during firing at 950 °C, which may be caused by a structural transformation and melting of halite, sylvine and their solid solution [51]. The reference mixture without ash (A-0) had a density of 1.89 g/cm^3, while the increased ash content decreased the density to 1.49 g/cm^3 for 15 wt% ash F1 (Table 4). This phenomenon is attributed to the pore-forming characteristics of the biomass ashes [52].

Fig. 3 depicts compressive and bending strength of fired bricks in relation to water absorption. The compressive strength, bending strength and water absorption of the pure clay-marl sample (sample A-0) at 950 °C were 72.6 MPa, 17.0 MPa and 11.8%. The reference compressive strength of 72.6 MPa is higher than the commercial values typically quoted for standard clay bricks (commonly 15–35 MPa for hollow bricks), which can be attributed to two factors: (i) the clay used in this study is of high plasticity, producing a particularly dense ceramic matrix upon firing [53]; and (ii) the laboratory-extruded cylinders tested here are solid and compact, unlike the perforated hollow blocks used in most commercial production, so the area under load is the full cross-section. The compressive

Table 4
Mixture properties at shaping and their relation to drying shrinkage, firing shrinkage and density. Abbreviations: F1-F4 = FA; B1-B4 = BA.

Mixture properties at:			shaping		drying	firing	
Sample	Ash	Ash content (wt %)	Pfeffer-korn	Moisture (% by dry mass)	Drying shrinkage by length (%)	Firing shrinkage by length (%)	Density (g/cm^3)
A-0	-	0	1.48	23.2	7.8	0.2	1.89
A-2		5	1.43	25.2	6.7	0.1	1.72
A-1	F1	10	1.45	27.6	5.6	0.2	1.63
A-3		15	2.22	33.2	6.8	0.1	1.49
A-4		5	1.60	26.2	7	0.2	1.73
A-5	B1	10	1.67	29.6	5.3	0.4	1.61
A-6		15	2.67	32.4	5.1	0.4	1.54
A-7	B2	5	1.60	26.2	6.9	0.5	1.7
A-8		10	2.67	30.6	6.4	0.6	1.62
A-9	B3	5	1.90	31.7	6.6	0.3	1.61
A-10		10	2.10	25.6	6.1	0.1	1.49
A-11	F3	5	1.82	27.6	6.8	0.3	1.71
A-12		10	2.35	31.7	6.7	0.2	1.58
A-13	F2	5	1.67	23.4	6.7	*samples disintegrated*	
A-14		10	1.74	22.2	5.8	*samples disintegrated*	
A-15	B4	5	1.74	30.9	4.8	0.8	1.54
A-17	F4	5	2.22	32.3	8	0.5	1.63
A-18		10	2.00	32.3	6.1	0.5	1.54

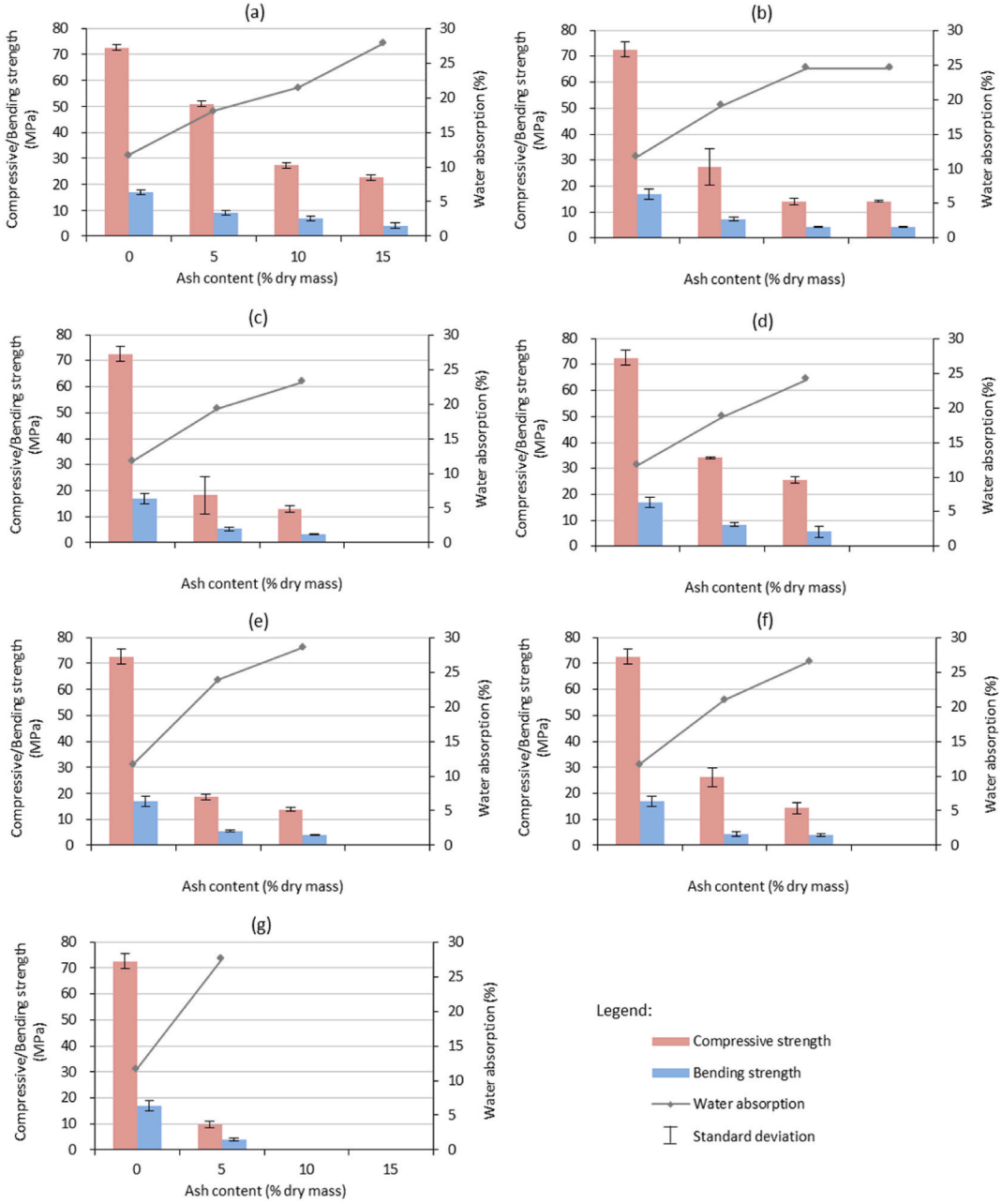

Fig. 3. Compressive/bending strength and water absorption for fired bricks with different ashes (Table 1): a) F1, b) B1, c) B2, d) F3, e) B3, f) F4, g) B4.

strength of perforated bricks decreases in proportion to the reduction in solid cross-sectional area [23,54,55]. As the clay-marl mixture was partly replaced by ash, an increased water absorption resulted in the significantly reduced compressive and bending strength. These findings are in agreement with existing studies [56]. However, except for the brick with 5 wt% paper sludge ash, all samples had compressive strengths above the 10 MPa limit specified in EN 772-1 [57]. To gain better insights into the reason for the decrease in strength, the brick microstructure was studied.

3.3. Effect of the ash content on the brick microstructure

The influence of the ash content on the brick microstructure was studied for the selected ash F1, which showed the smallest reduction in brick strength (Fig. 3), which is a critical parameter for brick production [58]. It should be noted that differences in mean compressive strength between adjacent replacement levels, particularly 5 and 10 wt%, may not be statistically significant given the

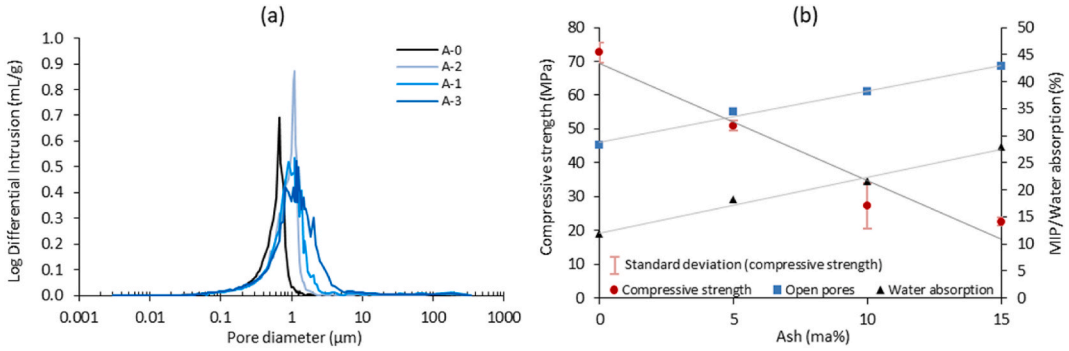

Fig. 4. (a) Log differential intrusion vs. pore size of the prepared brick specimens with various wt% of the ash F1: A-0 = 0 wt%; A-2 = 5 wt%; A-1 = 10 wt%; A-3 = 15 wt%. (b) Influence of the ash content on the compressive strength and open porosity.

observed variability (Fig. 4b). The main crystal phases in the fired bricks were quartz, feldspar, anhydrite and hematite (Supplement 2). The increased amount of ash had no significant effect on the amorphous content (Table 5).

The pore size distribution of open pores, as revealed by MIP, is shown in Fig. 4a. However, MIP measures the largest entrance of the pores and, due to the "bottleneck" effect, underestimates the pore diameter [27,59,60]. To get a more complete picture (e.g. closed pores, pores larger than 1 mm, cracks, etc.) it is combined with other methods, such as SEM [61]. The pore diameters and crack widths measured by SEM are shown in Table 6 and Fig. 5.

The pure clay-marl bricks had a total porosity of 28.2% according to MIP. After adding 5, 10, or 15 wt% of ash F1, porosity gradually increased, similarly as reported by Ref. [21]. The results were consistent with increased water absorption and decreased density (Table 4) and strength (Fig. 4b). As the ash content increased, the number of pores around 100 μm in diameter decreased, while larger pores became more common. Spherical, spheroidal, angular and rod-like pores [62] were identified. Spherical and spheroidal pores (aspect ratio <2) are attributed to gas bubble entrapment during mixture homogenisation and vacuum extrusion. Angular pores (aspect ratio 2-5) commonly reflect the decomposition of mineral grains (e.g., carbonates), while rod-like pores (aspect ratio 5-25) are linked to the burnout of elongated unburnt carbon particles from wood-derived ash, oriented parallel to the extrusion direction [52]. According to their orientation (Fig. 5d), cracks originated in the discontinuities such as slip lines and laminations within the plastic mass, which are formed by the translational and rotational movements of the clay particles during extrusion [25].

3.4. Influence of the ash type on the brick microstructure

The influence of the ash type on the brick microstructure was studied for the samples with 10 wt% ash, except for ash B4, where 5 wt% ash was studied (mixture A-15), since it was not possible to mould samples with a higher content of ash B4. However, according to the Pfefferkorn value the plasticity of A-15 was similar to that of the mixes with 10 wt% ash (Table 4). The main crystal phases in the fired bricks with 10 wt% ash were quartz, feldspar, anhydrite and hematite (Supplement 3). The quantitative phase composition, including amorphous content, is shown in Table 7.

Compared to other samples, bricks with MSW-SS ash had a significantly decreased amorphous content and an increased feldspar and hematite content, most likely due to the presence of NaCl, which lowered the temperature of mineral transformations [63]. The amorphous content of the bricks varied between 57 and 62 wt% with exception of A-14 (MSW-SS FA), where it was 30%. However, the amorphous content showed no correlation with the compressive strength of the bricks because at 950 °C vitrification has not yet occurred and the amorphous phase is related to the unreacted surplus of decomposed clay minerals [64].

The pore size distribution of open pores, as revealed by MIP, is shown on Fig. 6. Pores larger than 1 μm in diameter, potential closed

Table 5
Phase composition and amorphous content of fired bricks with 0, 5, 10 and 15 wt% ash F1, determined using a Rietveld refinement. Agreement indices: Rwp – weighteg R profile, GOF - goodness of fit.

	A-0	A-2	A-1	A-3
Ash F1 (wt%)	0	5	10	15
Quartz (wt%)	30.4	29.7	28.1	27.2
Plagioclase (wt%)	6.6	6.5	6.1	7.9
K-feldspar (wt%)	3.2	4.6	5.2	5.3
Hematite (wt%)	1.2	1.6	1.7	1.6
Iron sulfate (wt%)	<1.0	<1.0	<1.0	<1.0
Anhydrite (wt%)	<1.0	<1.0	<1.0	<1.0
Perovskite (wt%)	<1.0	<1.0	<1.0	/
Amorphous (wt%)	57.4	56.4	57.7	56.7
Rwp	4.2	4.3	4.4	4.4
GOF	2.3	2.3	2.4	2.3

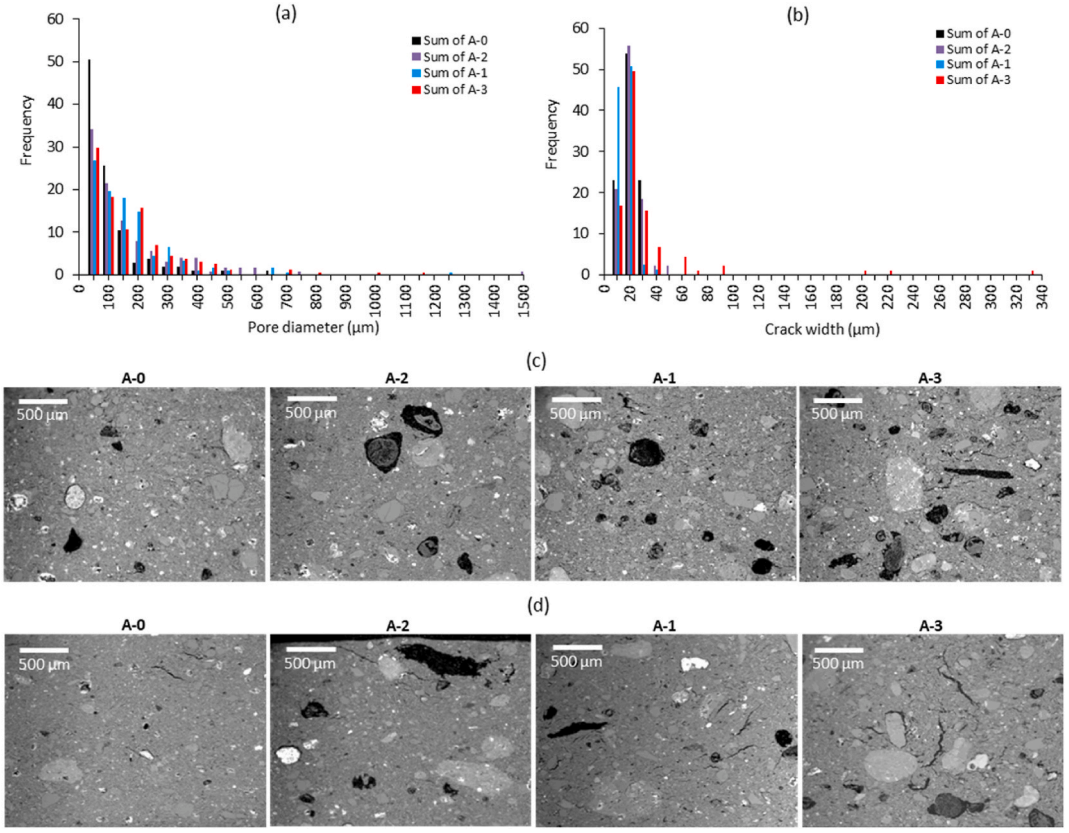

Fig. 5. Histograms of pore diameter (a) and crack width (b). Data were measured by SEM tools on brick specimens with 0 wt% (A-0), 5 ma % (A-2), 10 wt% (A-1) and 15 wt% (A-3) of the ash F1. For each shown specimen representative SEM micrographs of pores (c) and cracks in cross section parallel to extrusion (d) were evaluated.

pores and cracks, which were examined by SEM, are presented on Fig. 7 and Fig. 8. It should be noted that MIP may underestimate pore and crack dimensions due to the bottleneck effect and may not fully capture microcracks depending on their connectivity. SEM-based crack-width quantification was employed to explicitly capture microcracking features that may be missed or underestimated by MIP. After adding the ashes, the pore diameter and open porosity significantly increased, except for MSW-SS fly ash F2 (A-14). Bricks with BA had a higher open porosity than bricks with FA, with the exception of MSW-SS ash where the porosity of the bricks was similar independent of whether FA or BA was incorporated in the samples. This is probably related to a similar PSD of the ashes (Table 2). Wood BA (A-10) acted as a pore forming agent [52] with the highest increase in brick porosity (MIP and SEM). The lowest increase in open porosity (MIP) was documented for bricks made with MSW-SS BA (A-8). Bricks with BC-W FA showed the smallest reduction in strength, probably due to a higher degree of sintering [22,65,66].

Despite having the lowest porosity, bricks with the MSW-SS FA (A-14) cracked and disintegrated during firing. Bricks with BC, W, PS or MSWI ashes mostly had spherical, spheroidal and angular pores, while rod-like pores [62] were also common in bricks with W ash. These pores originated from elongated unburnt carbon particles [67].

Table 6
Porosity, measured by mercury intrusion porosimetry (MIP) and pore diameter/crack width, measured by scanning electron microscopy (SEM) tools for various mass % of the ash F1. Abbreviations: no. = number of data.

	Ash (wt %)	MIP			SEM – pore diameter					SEM – crack width				
		Porosity (%)	Average pore diameter (μm)	Average pore diameter - increase (%)	No.	Min (μm)	Max (μm)	Average (μm)	Average – increase (%)	No.	Min (μm)	Max (μm)	Average (μm)	Average – increase (%)
A-0	0	28.2	0.4	0	105	12.5	645.7	83.8	0	13	9.9	21.5	14.9	0
A-2	5	34.4	0.6	50	126	7.4	1486.0	147.8	76	43	5.5	45.8	15.5	4
A-1	10	38.2	0.7	75	183	5.2	1240.0	142.8	70	81	2.8	33.1	11.3	−24
A-3	15	42.8	0.7	75	158	10.7	1104.0	156.9	87	89	4.3	326.5	27.8	87

Negative values denote a reduction relative to A-0.

Table 7
Phase composition, amorphous content and compressive strength of bricks with 10 wt% of various ashes and reference A-0, determined by Rietveld method. Agreement indices: Rwp – weighteg R profile, GOF - goodness of fit. Fuel type abbreviations: BC = brown coal; W = wood; MSW = municipal solid waste; SS = sewage sludge; PS = paper sludge.* The maximum ash content allowing a proper shaping of A-15 was 5 wt%.

	A-0	A-1	A-5	A-8	A-10	A-12	A-14	A-15*	A-18
Ash	-	F1	B1	B2	B3	F3	F2	B4	F4
Fuel type for ash	-	BC-W	BC-W	MSW-SS	W	W	MSW-SS	PS	BC-W-PS
Quartz (wt%)	30.4	28.1	28.6	26.7	24.6	26.6	20.1	29.1	27.0
Plagioclase (wt%)	6.6	6.1	5.8	6.2	4.2	4.8	26.7	4.3	3.4
K-feldspar (wt%)	3.2	5.2	5.8	4.6	6.3	6.4	16.3	6.2	5.8
Hematite (wt%)	1.2	1.7	1.4	1.4	1.1	1.2	4.4	1.2	1.1
Iron sulfate (wt%)	<1.0	<1.0	1.1	<1.0	1.3	1.2	-	1.4	1.3
Anhydrite (wt%)	<1.0	<1.0	<1.0	<1.0	<1.0	<1.0	<1.0	<1.0	<1.0
Perovskite (wt%)	<1.0	<1.0	<1.0	<1.0	-	<1.0	<1.0	<1.0	<1.0
Halite (wt%)	-	-	-	-	-	-	<1.0	-	-
Amorphous (wt%)	57.4	57.7	57.4	59.5	62.1	59.2	30.5	57.3	61.1
Compressive strength (MPa)	72.6	27.3	14.2	12.9	13.9	25.7	disintegrated at firing	9.7	14.3
Rwp	4.2	4.4	4.7	4.4	3.1	4.4	3.6	5.0	4.6
GOF	2.3	2.4	2.5	2.3	2.3	2.3	1.9	2.6	2.4

Based on SEM observations the presumed predominant origin of the cracks was suggested (Table 9). Structures in bricks A-0 (without ash) were considered as a reference, with a minimal number of cracks. Although A-0 exhibited almost the largest drying shrinkage (Table 4), these cracks are unlikely to originate from drying. Specifically, these are subhorizontal in the P cross-section and inclined at approximately 30° from the top or bottom of the brick, whereas drying cracks are parallel structures that typically initiate at the top surface and propagate into the interior [68]. The cracks in A-0 most likely originate from extrusion-induced interlaminar tangential stress, which caused the alignment of irregular particles parallel to the slip [25]. Bricks with BC-W FA and BA showed a similar crack distribution to A-0, except that the deformation was more pronounced, especially in BA (Fig. 9), which required additional moisture to achieve adequate kneadability (Table 4). The influence of vacuum extrusion was evident from the specific geometry, indicating extensional deformation of the sample ([69], Supplement 4). In bricks with MSW FA large subvertical cracks are most probably associated with halite and sylvine decomposition (Fig. 1) related to high Cl content of ash F2 (Table 2). Namely, F2 contains 22.4 wt% Cl, 30.2 wt% Na_2O, and 3.8 wt% K_2O. At temperatures around 600 °C, the NaCl-KCl system forms a eutectic [70], resulting in a liquid phase trapped in the dense brick matrix. Above 800 °C, Cl salts release HCl gas [71], which probably accumulated in the bricks

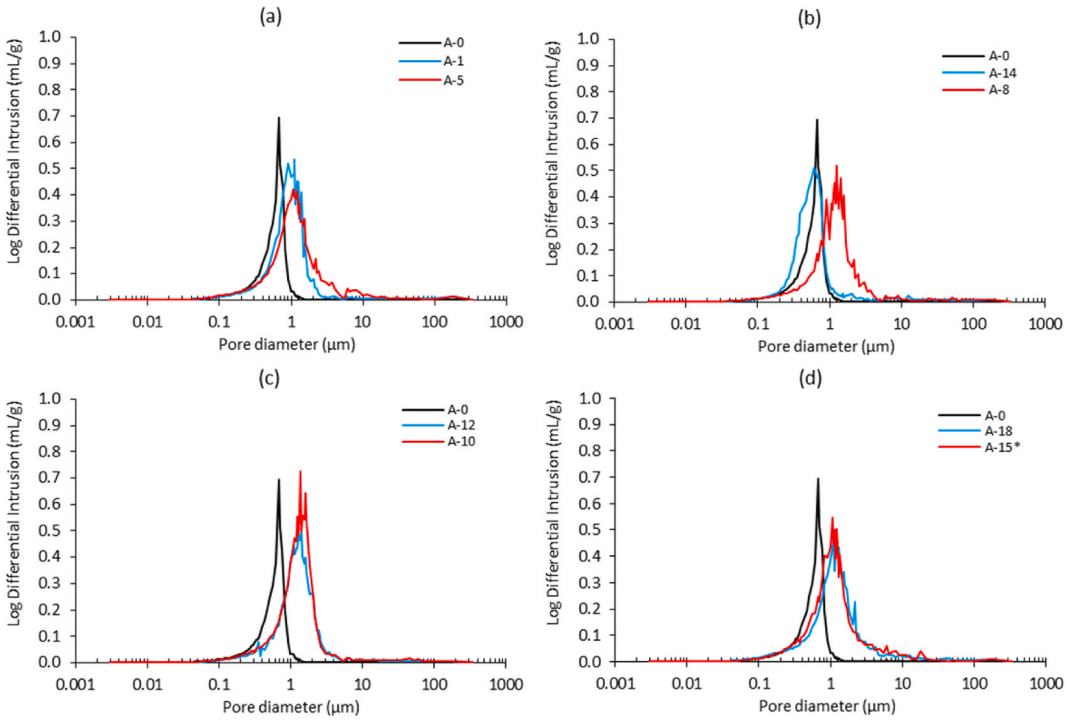

Fig. 6. Log differential intrusion vs. pore size of the prepared brick specimens with 10 wt% of various ashes: (a) F1 (A-1) and B1 (A-5); (b) F2 (A-14) and B2 (A-8); (c) F3 (A-12) and B3 (A-10); (d) F4 (A-18) and B-4 (A-15*). * The maximum ash content, which allowed proper shaping was 5 wt% (A-15).

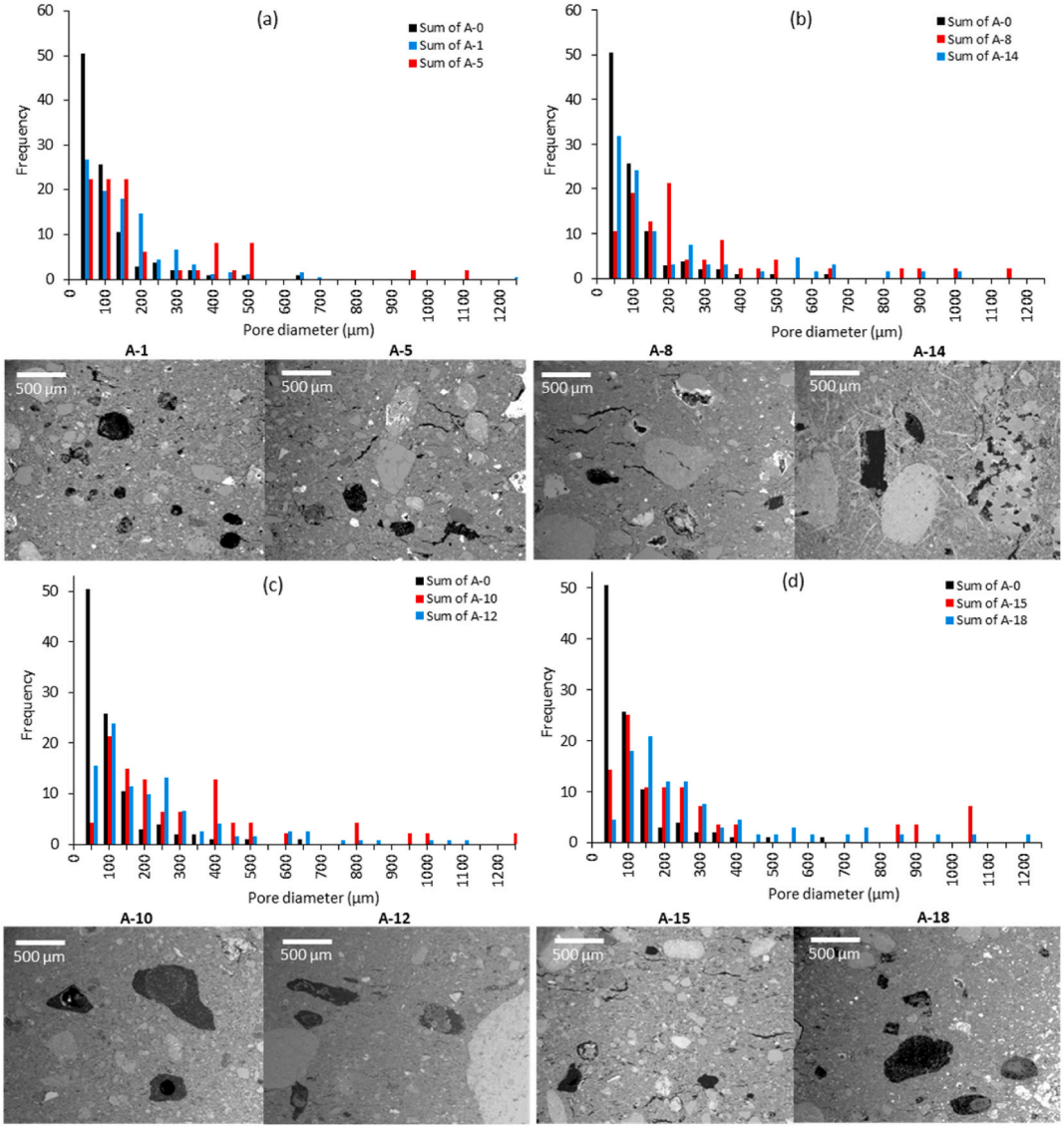

Fig. 7. Frequency distribution of pore diameter for data, measured by SEM tools on brick specimens with 10 wt% of various ashes: (a) F1 (A-1) and B1 (A-5); (b) F2 (A-14) and B2 (A-8); (c) F3 (A-12) and B3 (A-10); (d) F4 (A-18) and B-4 (A-15*). * The maximum ash content, which allowed proper shaping was 5 wt% (A-15*). For each specimen are shown representative SEM micrographs of pores.

with a dense structure and small pore diameter, generating internal stresses that led to crack formation. In bricks with MSW BA, large subhorizontal cracks formed, probably primarily due to increased clay alignment related to the high water demand of the mixture (Table 4). Volume changes related to the α-β quartz phase transformation [72] and calcite calcination [73] during firing at 950 °C may also contribute to cracking (Fig. 1, Table 2, Supplement 5). During vacuum extrusion, in bricks with both types of wood ash, elongated unburnt carbon particles within the plastic mixture were oriented parallel to the clay alignment and formed weakened areas, which are connected by subparallel cracks (Supplement 6). Similar conclusions have been reported for bricks with sawdust, where larger pores acted as more intense crack initiation sites, drastically reducing the compressive strength of the samples [74]. In bricks with PS ash, cracks most commonly formed near carbonate and quartz clasts (Fig. 1, Table 2, Supplement 7). PS mixtures required very high moisture to achieve adequate kneadability (Table 4), which accelerated clay alignment during extrusion (Fig. 8). Subordinately, it may be induced by α-β quartz [72] and calcite-lime transformation [73], similar to that in bricks with MSW-SS BA.

Porosity was identified as the primary parameter influencing strength reduction. The compressive strength of bricks containing different ashes was negatively correlated with MIP porosity, maximum pore diameter, and average pore diameter (Fig. 9a). Similarly, the average crack width showed a negative correlation with compressive strength (Fig. 9c). However, MSW-SS ash was an outlier, exhibiting a significantly higher average crack width but a similar compressive strength to other BA (Fig. 9c). The Pearson correlation coefficient between MIP porosity and compressive strength (all data) is $r = -0.94$. When MSW-SS samples are excluded, this improves

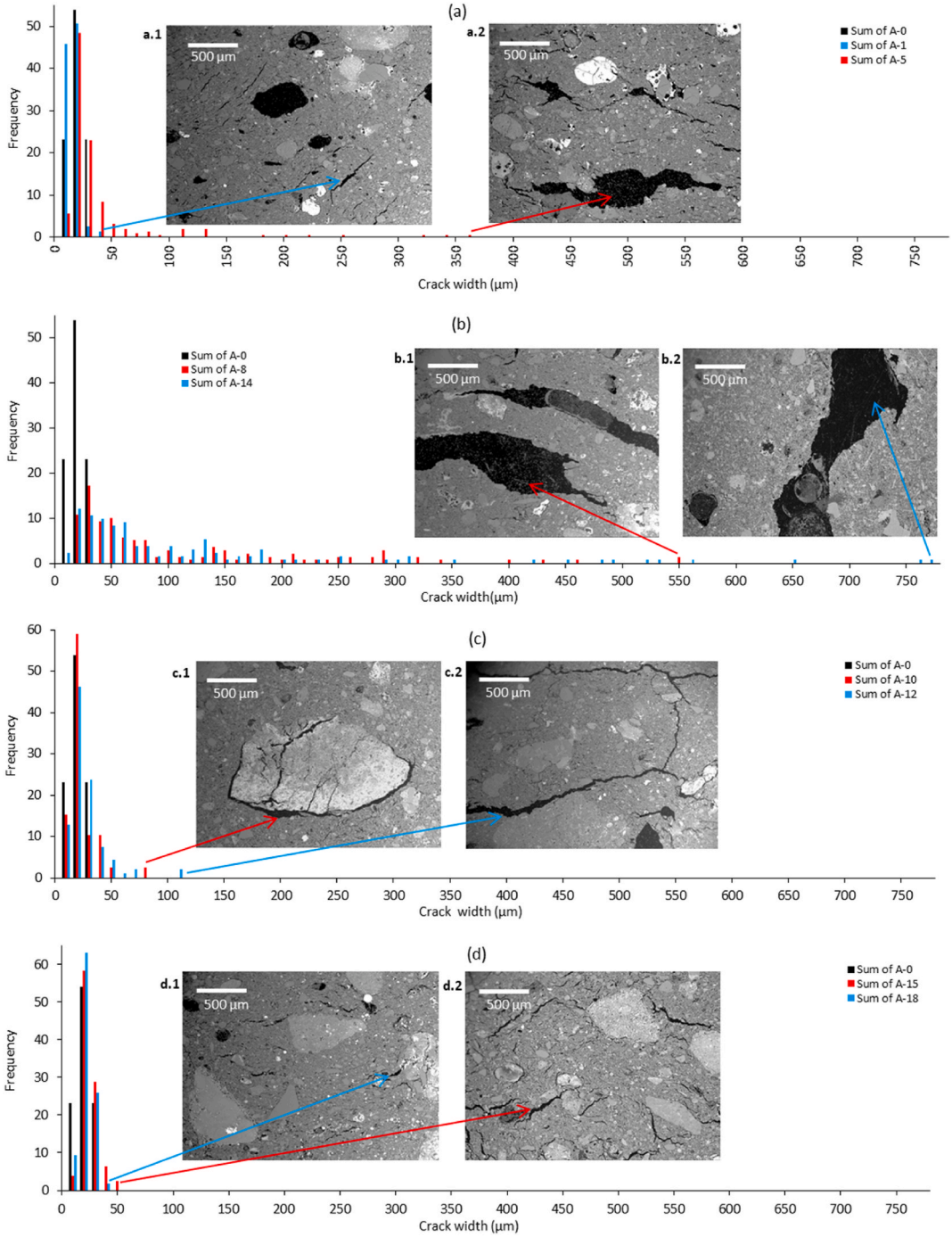

Fig. 8. Histograms of crack width, measured by SEM on brick specimens with 10 wt% of various ashes: (a) F1 (A-1) and B1 (A-5); (b) F2 (A-14) and B2 (A-8); (c) F3 (A-12) and B3 (A-10); (d) F4 (A-18) and B-4 (A-15*). * The maximum ash content, which allowed proper shaping was 5 wt% (A-15*). For each specimen are shown representative SEM micrographs of cracks. The effects on crack development were evaluated by comparison with the reference mix A-0.

to r = −0.98. The corresponding values for average pore diameter vs. strength are r = −0.86 (all) and r = −0.85 (excluding MSW-SS). These values are confirming that the porosity-strength model is robust for most ash types and that the salt-rich MSW-SS ashes represent a mechanistically distinct sub-class. Considering the influence of porosity on the compressive strength of bricks, it can be observed that among bricks with porosity around 38%, those with MSW-SS BA (A-8) showed significantly reduced compressive strength compared to bricks with BC-W FA (A-1) and W FA (A-12) (Table 9, Fig. 9). This is most likely related to increased firing shrinkage (Table 4) and

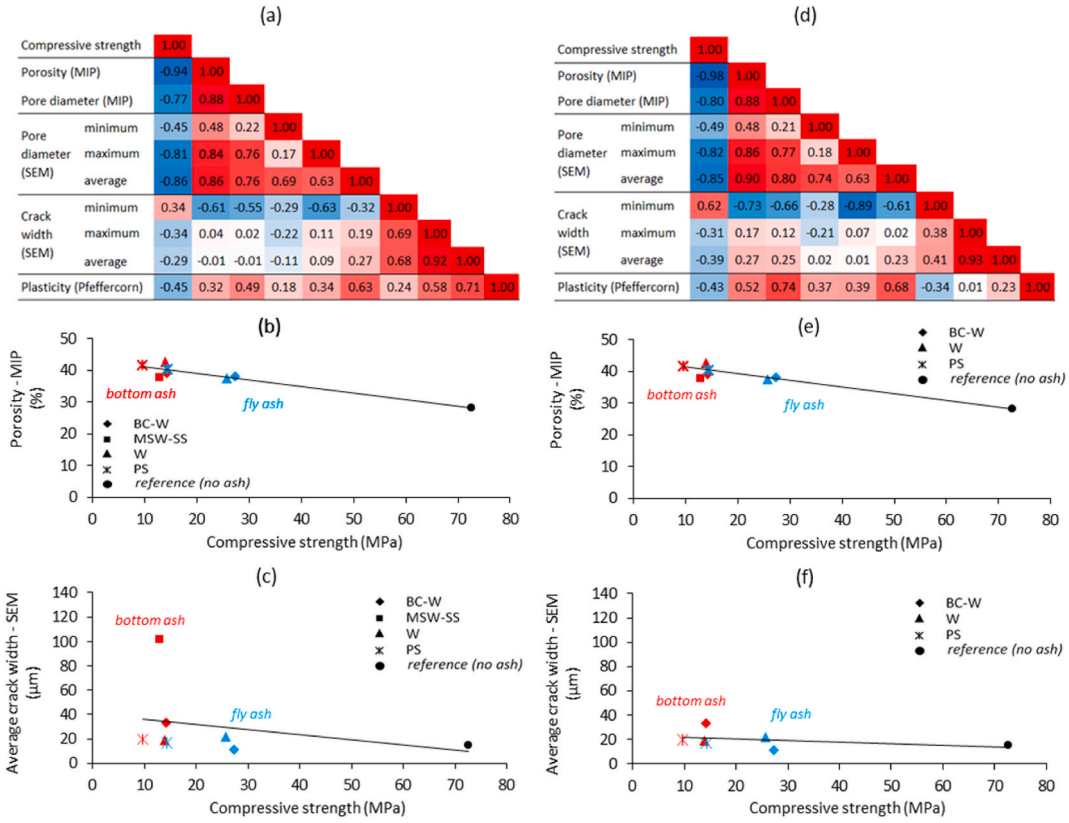

Fig. 9. The influence of the pore diameter and crack width of bricks with various ashes on their compressive strength: correlation matrix for all data, porosiy determined by MIP, and crack width determined by SEM for all ashes(a-c) and with excluded MSW-SS bottom ash (d-f).

Table 8
Evaluation of the effects on crack development for various biomass ashes, based on the results of SEM, XRD, drying shrinkage and firing shrinkage. Abbreviations: BC = brown coal; W = wood; MSW = municipal solid waste; SS = sewage sludge; PS = paper sludge; FA = fly ash; BA = bottom ash.

Fuel type	Ash type	Effects on crack development			
		Clay aligning during vacuum extrusion	Drying	Firing at 950 °C	Presumably predominant origin of cracks (schematic diagrams)
		SEM (Figs. 7 and 8, Supplement 4-7)	Drying shrinkage (Table 4)	Firing shrinkage (Table 4)	
Reference:	*No ash*	low	low	low	clay aligning (a)
BC-W	FA	low	low	low	clay aligning (a)
	BA	medium	low	low	clay aligning (a)
MSW-SS	FA	low	low	very high	salt decomposition (b)
	BA	medium	low	high	clay aligning (a) and mineral transformation (d)
WA	FA	medium	low	low	oriented elongated pores (c)/clay aligning (a)
	BA	high	low	low	oriented elongated pores (c)/clay aligning (a)
PS-SS	FA	medium	low	medium	clay aligning (a) and mineral transformation (d)
	BA	medium	low	very high	clay aligning (a) and mineral transformation (d)
Schematic diagrams:		(a) 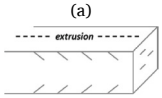	(b) 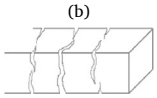	(c) 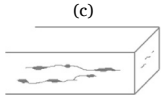	(d) 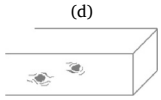

consequently increased average crack diameter (Table 8) in bricks A-8. The compressive strength of bricks with FA was generally higher than when BA was added (Fig. 9b), which is probably related to the higher packing density of fly ash compared to bottom ash [75]. The tertiary role in strength reduction was attributed to ash mineralogy; specifically, ashes with high CaO content (formed by calcite calcination above 900 °C) cause localised volume expansion, promoting crack nucleation near Ca-rich clasts.

3.5. Leaching behaviour of the fired bricks with ashes

Leaching tests were performed to evaluate the environmental impact of the prepared bricks in accordance with standard procedures. In Slovenia, the assessment of recycled or waste-derived materials for reuse is guided by the national Decree on Waste [76]. However, to enable comparison with European legislation applicable in all EU countries, all concentrations in this study are compared with the limit values for inert and non-hazardous waste specified in the Decree on Waste Landfill [77]. The tests quantified the mobility of relevant toxic substances and ensured that the materials meet the criteria established for their intended application or disposal. It should be noted, however, that leaching analysis of brick samples is not required when no secondary raw materials are added.

First, raw mineral wastes (ashes) were tested to determine which sample leached more toxic elements. Then, brick samples were tested and compared with the original sample without ash addition and with regulatory limits for inert and non-hazardous waste. pH values of CaO-rich ashes of all samples are above 12, except for sample F2, which has a pH of about 10.5 (Table 10). As shown in Table 10, some waste ashes contain higher concentrations of potentially toxic elements, for example, sample F2 (MSW-SS FA). Ni, Cu, Zn, Cd and Hg did not exceed the limit values for inert waste in the raw materials. However, Cr is above the limit values for inert waste in samples B2, B3, F2 and F3, with B3 and F2 even exceeding the limit values for non-hazardous waste. As is above the limit values for inert waste in sample F2; Se in samples F2 and F3; Mo in samples F2, F3 and B3; and Pb in samples B2 and F4. Sb is above the limit values for inert waste in sample B2 and above the limit for non-hazardous waste in sample F2. Ba is the toxic element most frequently present above the limit values for inert waste in the raw materials (samples F1, F3, F4, B2, B3 and B4), and above the limit values for non-hazardous waste in sample F4. Sample F2 contains a high amount of Na and Cl (XRF data in Table 2), and sylvine was identified by XRD analysis (Fig. 1). The leaching of toxic elements may be associated with the presence of Cl^- (or NaCl), which can be readily washed out and may thereby contribute to the mobility of these elements. The release of As could be facilitated by NaCl [78] and as seen in Tables 10 and in sample F2, As is significantly higher than in other raw materials.

Although fired bricks are typically considered inert construction materials, in this study the bricks incorporated up to 15 wt% of various ashes (brown coal, wood, municipal solid waste, sewage sludge, and paper sludge) and were tested for potential end-of-life scenarios where environmental leaching could be relevant. Similar than for raw materials, leaching tests were conducted according to EN 12457 [41] to assess the mobility of toxic elements under conditions relevant for waste assessment (L/S = 10, particle size < 4 mm), a method widely used in regulatory frameworks across Europe, including national waste assessment procedures. The use of a single standardised ratio is sufficient to assess environmental relevance within the scope of this study. The objective was not to model detailed time-dependent leaching kinetics, but to ensure comparability with existing regulatory criteria and published literature.

Table 10 shows the concentrations of toxic elements leached from different mixtures of bricks, with and without added ashes. In addition, pH values for all mixtures were provided, with ash-clay bricks showing a pH above 11 (Table 10) in all mixtures except for samples A-13 and A-14, which had lower pH values of around 8 and 9, respectively. The reference mixture A-0 did not show elevated levels of toxic elements according to national and EU legislation for inert waste [77]. Leaching results for extruded bricks with addition

Table 9
Porosity, measured by MIP and pore diameter/crack width, measured by SEM for bricks with 10 wt% of various ashes (*the maximum ash content, which allowed proper shaping was 5 wt%). Abbreviations: BC = brown coal; W = wood; MSW = municipal solid waste; SS = sewage sludge; PS = paper sludge; FA = fly ash; BA = bottom ash.

	Fuel type for ash	MIP			SEM – pore diameter					SEM – crack width				
		Porosity (%)	Average pore diameter (μm)	Average pore diameter - increase (%)	No.	Min (μm)	Max (μm)	Average (μm)	Average – increase (%)	No.	Min (μm)	Max (μm)	Average (μm)	Average – increase (%)
A-0	-	28.2	0.4	0	105	12.5	645.7	83.8	0	13	9.9	21.5	14.9	0
A-1	BC-W (FA)	38.2	0.7	75	183	5.2	1240.0	142.8	70	81	2.8	33.1	11.3	−24
A-5	BC-W (BA)	39.2	0.7	75	49	16.0	1052.0	190.4	127	217	8.3	352.8	33.4	124
A-8	MSW-SS (BA)	37.6	0.7	75	47	17.4	1104.0	249.4	198	139	11.3	545.0	102.2	586
A-10	W (BA)	42.8	0.9	125	47	26.0	1208.0	287.5	243	39	2.8	71.5	19.1	28
A-12	W (FA)	38.9	0.9	125	122	13.8	1093.0	211.9	153	93	5.7	107.7	22.0	48
A-14	MSW-SS (FA)	37.8	0.5	25	66	1.1	1219.0	194.8	132	131	6.1	767.2	116.1	679
A-15*	W-PS (BA)	41.7	0.8	100	28	33.2	1022.0	256.7	206	156	5.5	45.1	19.8	33
A-18	BC-W-PS (FA)	40.5	0.7	75	67	46.8	1152.0	264.5	216	54	3.9	31.4	16.9	13

Negative values denote a reduction relative to A-0.

Table 10
Leaching results of raw materials and extruded bricks with different ashes and the reference sample. Bolded values indicate results above limiting values for inert waste. Fuel abbreviations: C = clay; F1, F2, F3, F4 = fly ashes; B1, B2, B3, B4 = bottom ashes; BC = brown coal; W = wood; MSW = municipal solid waste; SS = sewage sludge; PS = paper sludge.

	ash/fuel	ash (wt%)	Cr (mg/kg)	Ni (mg/kg)	Cu (mg/kg)	Zn (mg/kg)	As (mg/kg)	Se (mg/kg)	Mo (mg/kg)	Cd (mg/kg)	Sb (mg/kg)	Ba (mg/kg)	Hg (mg/kg)	Pb (mg/kg)	pH (25 °C)
C			0.011	0.005	0.012	<0.002	<0.001	0.026	0.041	<0.002	0.002	0.086	<0.001	<0.005	10.18
F1	BC-W		0.037	0.009	0.003	0.041	0.003	0.023	0.172	<0.002	<0.001	**26.74**	<0.001	0.026	12.87
B1	BC-W		0.143	0.014	0.008	0.005	0.002	0.017	0.066	<0.002	<0.001	15.97	<0.001	0.196	12.95
B2	MSW-SS		**0.696**	0.011	1.165	2.823	0.002	0.021	0.376	<0.002	**0.157**	**94.61**	<0.001	**3.577**	12.72
B3	W		**13.83**	0.006	0.039	0.312	<0.001	0.053	**0.801**	0.002	0.002	14.49	<0.001	0.021	13.46
F3	W		**8.671**	0.051	0.565	1.863	0.007	**0.134**	**1.017**	0.003	0.013	9.674	<0.001	0.169	13.01
F2	MSW-SS		**33.67**	0.004	0.016	<0.002	**2.344**	**1.942**	**6.762**	0.005	**71.43**	0.045	0.007	0.029	10.52
B4	BC-W-PS		0.018	0.01	0.185	0.095	<0.001	0.016	0.017	<0.002	0.004	**96.14**	<0.001	0.401	12.96
F4	BC-W-PS		0.014	0.007	0.08	1.573	<0.001	<0.003	0.079	<0.002	0.005	**235.2**	0.002	**2.438**	12.33
A-0	-	-	0.139	0.006	0.002	0.002	0.237	0.036	0.442	<0.002	0.005	0.583	0.009	<0.005	12.09
A-2	F1/BC-W	5	0.343	0.003	<0.001	0.007	0.201	0.090	**0.511**	<0.002	0.005	0.255	0.002	<0.005	11.95
A-1		10	0.380	0.003	<0.001	0.015	0.252	**0.104**	**0.660**	<0.002	0.010	0.277	0.002	<0.005	11.54
A-3		15	**0.621**	0.003	<0.001	0.002	0.202	0.028	**0.740**	<0.002	0.007	0.502	<0.001	<0.005	11.70
A-4	B1/BC-W	5	0.381	<0.002	<0.001	0.004	0.012	0.025	0.413	<0.002	<0.001	0.458	0.001	<0.005	12.34
A-5		10	**0.719**	<0.002	<0.001	<0.002	0.004	0.026	0.330	<0.002	<0.001	0.165	<0.001	<0.005	12.37
A-6		15	**1.163**	0.004	<0.001	<0.002	0.001	0.039	0.312	<0.002	<0.001	0.225	<0.001	<0.005	12.48
A-7	B2/MSW-SS	5	**0.566**	0.002	<0.001	0.013	0.238	0.031	**0.573**	<0.002	**0.088**	0.260	0.001	<0.005	11.59
A-8		10	**0.920**	0.003	0.002	0.002	0.151	0.019	**0.791**	<0.002	**0.095**	0.279	0.001	<0.005	11.16
A-9	B3/W	5	**0.816**	<0.002	<0.001	<0.002	0.004	0.015	0.377	<0.002	<0.001	0.486	<0.001	<0.005	12.28
A-10		10	**2.107**	<0.002	<0.001	<0.002	<0.001	0.020	0.357	<0.002	<0.001	0.579	<0.001	<0.005	12.45
A-11	F3/W	5	0.363	0.002	<0.001	<0.002	0.103	0.037	0.397	<0.002	0.004	0.246	<0.001	<0.005	12.03
A-12		10	**0.717**	0.002	<0.001	<0.002	0.067	0.033	0.448	<0.002	0.002	0.325	<0.001	<0.005	11.86
A-13	F2/MSW-SS	5	0.130	0.025	<0.001	<0.002	**0.726**	<0.003	**0.765**	<0.002	0.023	0.085	<0.001	<0.005	7.92
A-14		10	**0.690**	0.038	<0.001	0.012	**0.781**	<0.003	**1.267**	<0.002	0.011	0.939	<0.001	<0.005	8.81
A-15	B4/W-PS	5	**1.253**	<0.002	<0.001	0.003	<0.001	0.013	0.362	<0.002	<0.001	0.277	<0.001	<0.005	12.41
A-17	F4/BC-W-PS	5	**0.520**	<0.002	<0.001	<0.002	0.154	0.032	**0.573**	<0.002	0.002	0.403	0.003	<0.005	11.76
A-18		10	0.869	0.007	<0.001	<0.002	0.021	0.025	**0.683**	<0.002	<0.001	0.726	0.002	<0.005	11.70
Inert waste[a]			0.5	0.4	2.0	4.0	0.5	0.1	0.5	0.04	0.06	20.0	0.01	0.5	/
Non-hazardous waste[a]			10.0	10.0	50.0	50.0	2.0	0.5	10.0	3	0.7	100.0	0.20	10.0	/

[a] European Decree on the waste landfill.

of different ashes show elevated concentrations of Cr, As, Mo, and Sb.

Chromium is a toxic element that exceeds the limit values for inert waste in almost all extruded brick samples with added ashes, except in samples A1, A2, A4, A11, and A13. Although the samples exceeded inert-waste limits, their leaching behaviour remains compatible with non-hazardous classifications. Waste-acceptance decisions under 2003/33/EC are formally based on total Cr; however, regulations based solely on total Cr may misrepresent actual risk, and due to the higher toxicity of Cr(VI), specific Cr(VI) limits are needed [79] e.g. bricks and tiles mainly release Cr as Cr(III), whereas some mixed recycled aggregates mainly release Cr(VI) [80]. Chromium leaching from bricks is mainly controlled by how Cr is incorporated into the ceramic matrix and by the glassy phase formed during [81–83].

Free lime (CaO) in ash promotes high-temperature oxidation of Cr(III) [84] and the formation of solid chromates such as $CaCrO_4$, increasing the Cr(VI) fraction and its potential leachability in alkali solutions. At high alkali pH, Cr is mainly present and leached as chromate (Cr(VI)), with its concentration controlled by Ca-chromate and other Ca–Al–Cr(VI) [85–87] phases.

Leaching of As occurs only in samples where ash F2 (MSW-SS FA) was added. Leaching of As from MSW SS bricks is controlled by the As content and speciation in the raw materials, as well as by firing-induced changes in phase and porosity, rather than solely by the stability of the final mineral structure. In case of Sb, only the bricks containing B2 ash exhibited elevated Sb leaching. B2 show elevated concentrations even when performing leaching test for raw materials. Sb leaching is strongly linked to the bottom ash chemistry and Ca–Sb phases. This is consistent with literature reporting that Sb in MSWI bottom ash is mainly present in Ca–antimonate phases (romeite) whose dissolution, especially under reduced Ca or carbonation, controls Sb(V) release, making Sb the critical element in bottom-ash based construction materials [88–90].

However, the F2 raw material, which contains a significantly high concentration of Sb in leachate, shows no leaching after being added to the clay mixture. There is strong leaching when alone, but once co-fired with clay, Sb is chemically incorporated and physically encapsulated in a denser ceramic matrix, so leaching can fall below the limit values for inert waste even though the total Sb in the brick remains high. Also very efficient immobilisation in fired bricks has been found for Ba, where the raw materials show high concentrations in almost all samples except B1 and F2.

Mo often remains mobile and leachable in bricks [91], largely independent of added ash (samples A1–A3, A7, A8, A13, A14, A17, and A18). In alkaline pore solutions (typical for ashes and many ceramics or binders), Mo is present mainly as molybdate (MoO_4^{2-}), a highly soluble oxyanion [92–94]. Similarly to Cr, in clay ceramics with industrial wastes, Cr and Mo are the only elements not fully immobilised after firing; their leaching depends on the amount of glassy phase and mixture basicity rather than just the total Mo content [81]. For coal-waste fired bricks, most toxic elements are strongly immobilised after firing, but Mo shows a distinct trend and can remain more mobile [91]. It follows that elevated Mo in raw materials and bricks likely reflect the oxyanion chemistry of Mo: it remains as soluble molybdate, controlled by matrix pH and glass or mineral phases, so firing and ash addition that immobilise, for example, Ba and Sb do not necessarily reduce Mo leaching. Adjusting mixture basicity, glass content, or adding specific Mo-stabilising phases would be needed to change this behaviour.

In summary, the required properties of fired clay bricks depend on their intended use. For masonry units, the European standard [57] prescribes a compressive strength of 10 MPa. All prepared mixtures produced from the clay investigated in this study met this criterion, except for bricks containing W-PS BA, where incorporating 5 wt% of ash resulted in a slightly lower compressive strength. Because the interaction between clay raw materials and additives is highly material-specific, the effect of the additive cannot be generalized and must be experimentally reassessed for each clay source and additive dosage. Generally high plasticity clay, as in present study, can accommodate higher amount of ash additives. Since the masonry units are covered by plaster and are not exposed to wet environments, leaching tests are not required and brick factories are not obligated to perform them. However, considering that brick buildings will eventually be demolished and the waste bricks will end up in landfill, information on the influence of ashes on the leaching behaviour of bricks is important. In the EU, the management of waste construction materials is prescribed by the Landfill Directive and national legislation. According to the Landfill Directive, all bricks are classified as non-hazardous waste, while bricks containing 5 wt% BC-W BA and 5 wt% W FA also meet the criteria for inert waste (Table 10).

For industrial applications, scaling effects should be considered, such as extrusion pressure, sample shape, and size. Industrial extrusion operates at higher pressure, which may influence the degree of clay particle alignment, lamination density, and reduce extrusion-related cracking. Conversely, small laboratory cylinders may exhibit higher compressive strength than large masonry units.

4. Conclusions

This study aimed to investigate the feasibility of reusing biomass ash (wood or wood co-combusted with coal), ash from co-combustion of SS and MSW incineration, and ash from co-combustion of coal, biomass and PS in the production of extruded clay bricks. The physical and mechanical properties, microstructure, and leaching behaviour of bricks containing 5, 10 or 15 wt% ash fired at 950 °C were evaluated. Based on extensive experimental data, the following conclusions can be drawn.

While ash incorporation generally reduced strength, a 15 wt% substitution met the 10 MPa standard for most ashes, except for Paper Sludge Bottom Ash (B4), where even 5 wt% substitution yielded marginally lower strength (9.7 MPa). The best mechanical performance was achieved by incorporating 5 wt% BC-W biomass ash, resulting in a compressive strength of 51 MPa. The main parameters responsible for lower compressive strength values were: (i) increased clay alignment, related to the higher water demand of mixtures with non-plastic ashes; (ii) increased porosity, as ashes acted as pore-forming additives; (iii) excessive CaO content due to calcite decomposition; (iv) cracks (crack width); and (v) particle size of ashes (finer ashes resulted in denser bricks with higher compressive strengths). Ashes reduced the drying shrinkage of bricks. Particle size also played a crucial role in reducing drying shrinkage, which was lower for coarser BA than for FA. The type of ash determined the predominant mechanism of crack development.

Ashes with high NaCl + KCl content (here, F2 MSW-SS FA with approx. 22 wt% Cl, 30 wt% Na_2O and 4 wt% K_2O) are incompatible with firing at 950 °C under the conditions tested: the formation of a eutectic liquid below 700 °C and HCl gas release above 800 °C caused catastrophic disintegration of all specimens. Industry should exercise extreme caution when considering high-salt ashes without prior pre-treatment (e.g., water washing).

All produced bricks comply with EU non-hazardous waste landfill criteria under EN 12457-2 standard procedure conditions. Notably, bricks incorporating 5 wt% BC-W BA (A-4) and 5 wt% W FA (A-11) also meet the stricter inert waste limits. Leaching behaviour for Cr, Ni, Cu, Zn, As, Se, Mo, Cd, Sb, Ba, Hg, and Pb was discussed. It is important to note that leaching performance is strongly ash-chemistry-dependent; in particular, Cr and Mo remained comparatively mobile across most brick compositions, controlled by their oxyanion speciation and the alkalinity of the ceramic matrix, even when other heavy metals were effectively immobilised by firing relative to inert and non-hazardous waste limit values under EN 12457-2 test conditions (L/S = 10, 24 h agitation, particle size <4 mm).

The study enables direct comparison of the influence of eight different types of ashes on the characteristics of extruded fired bricks. It offers a unified basis for better understanding of the relationships between the chemical and mineralogical properties of ash on the one hand, and the physical, mechanical, microstructural and leaching properties of extruded fired bricks with incorporated ash on the other. Such knowledge is a crucial step towards establishing broader implementation of the circular economy in the brick industry, which can make an important contribution to global zero-waste goals.

CRediT authorship contribution statement

Lea Žibret: Writing – review & editing, Writing – original draft, Validation, Resources, Methodology, Investigation, Formal analysis, Data curation. **Majda Pavlin:** Writing – review & editing, Investigation, Formal analysis. **Vilma Ducman:** Writing – review & editing, Supervision, Project administration, Methodology, Funding acquisition, Conceptualization.

Declaration of competing interest

The authors declare that they have no known competing financial interests or personal relationships that could have appeared to influence the work reported in this paper.

Acknowledgements

This research has been funded by the European Union under the AshCycle project, grant agreement no. 101058162, and partially supported by the Slovenian Research and Innovation Agency (ARIS) under research core grant no. P2-0273. The authors would like to thank Roman Maček for carrying out the ceramic technological tests and Dušica Tauzes and Mojca Škerl for technical support.

Appendix A. Supplementary data

Supplementary data to this article can be found online at https://doi.org/10.1016/j.jobe.2026.116371.

Data availability

Data will be shared on repository DIRROS at http://hdl.handle.net/20.500.12556/DiRROS-29414.

References

[1] K. Wang, J.W. Tester, Sustainable management of unavoidable biomass wastes, Green Energy Resour. 1 (2023), https://doi.org/10.1016/j.gerr.2023.100005.
[2] S. Lawanwadeekul, P. Chindaprasirt, A. Phumiphan, A. Srisuwan, N. Phonphuak, Transforming industrial waste by utilizing fly ash and bottom ash for sustainable clay bricks, J. Mater. Cycles Waste Manag. 27 (2025), https://doi.org/10.1007/s10163-025-02299-0.
[3] I. Carević, M. Serdar, N. Štirmer, N. Ukrainczyk, Preliminary screening of wood biomass ashes for partial resources replacements in cementitious materials, J. Clean. Prod. 229 (2019), https://doi.org/10.1016/j.jclepro.2019.04.321.
[4] M. Ishaq, A. Ali, A.A. Hussain, K. Kamran, A. Ghuffar, A. Anwar, Industrial waste as clay substitute in brick manufacturing, Constr. Build. Mater. 477 (2025), https://doi.org/10.1016/j.conbuildmat.2025.141359.
[5] R. Bunge, Recovery of metals from waste incinerator bottom ash2016. http://vbsa.ch/wp-content/uploads/2016/07/Studie-Bunge-Internetversion.pdf, 2016. (Accessed 24 May 2024).
[6] S. Petzet, B. Peplinski, S.Y. Bodkhe, P. Cornel, Recovery of phosphorus and aluminium from sewage sludge ash by a new wet chemical elution process (SESAL-Phos-recovery process), Water Sci. Technol. 64 (2011), https://doi.org/10.2166/wst.2011.682.
[7] S.V. Vassilev, C.G. Vassileva, Contents and associations of rare earth elements and yttrium in biomass ashes, Fuel 262 (2020), https://doi.org/10.1016/j.fuel.2019.116525.
[8] J. Heinimö, M. Junginger, Production and trading of biomass for energy – an overview of the global status, Biomass Bioenergy 33 (2009), https://doi.org/10.1016/j.biombioe.2009.05.017.
[9] B. Milovanović, N. Štirmer, I. Carević, A. Baričević, Wood biomass ash as a raw material in concrete industry, JCE 71 (2019), https://doi.org/10.14256/JCE.2546.2018.
[10] Z. Zhang, Y. Wang, Y. Zhang, B. Shen, J. Ma, L. Liu, Stabilization of heavy metals in municipal solid waste incineration fly ash via hydrothermal treatment with coal fly ash, Waste Manage. (Tucson, Ariz.) 144 (2022), https://doi.org/10.1016/j.wasman.2022.03.022.

[11] G.M. Kirkelund, P.E. Jensen, L.M. Ottosen, K.B. Pedersen, Comparison of two- and three-compartment cells for electrodialytic removal of heavy metals from contaminated material suspensions, J. Hazard Mater. 367 (2019), https://doi.org/10.1016/j.jhazmat.2018.12.063.
[12] Z. Zhang, Y. Yu, Y. Rao, Y. Wang, C. Yu, Z. Luo, H. Zhao, A. Saffarzadeh, X. Wang, C. Wu, Q. Wang, Stabilization of heavy metals in municipal solid waste incineration fly ash using organic chelating agents: insight into risk assessment and function mechanism, Sci. Total Environ. 914 (2024), https://doi.org/10.1016/j.scitotenv.2024.169986.
[13] Z. Haiying, Z. Youcai, Q. Jingyu, Utilization of municipal solid waste incineration (MSWI) fly ash in ceramic brick: product characterization and environmental toxicity, Waste Manage. (Tucson, Ariz.) 31 (2011), https://doi.org/10.1016/j.wasman.2010.10.017.
[14] A. Ukwatta, A. Mohajerani, Leachate analysis of green and fired-clay bricks incorporated with biosolids, Waste Manage. (Tucson, Ariz.) 66 (2017), https://doi.org/10.1016/j.wasman.2017.04.041.
[15] A.C. Pereira, Plasticity of Clays for Red Ceramics: the Role of Additives, Processing, and Ionic Interactions (2020–2025 Review), vol. 9, EMSJ, 2025, https://doi.org/10.59573/emsj.9(6).2025.9.
[16] G.M. Kirkelund, L. Skevi, L.M. Ottosen, Electrodialytically treated MSWI fly ash use in clay bricks, Constr. Build. Mater. 254 (2020), https://doi.org/10.1016/j.conbuildmat.2020.119286.
[17] A. Detho, A.A. Kadir, S. Ahmad, Utilization of wastewater treatment sludge in the production of fired clay bricks: an approach towards sustainable development, Results Eng. 21 (2024), https://doi.org/10.1016/j.rineng.2023.101708.
[18] L.M. Ottosen, I.M.G. Bertelsen, P.E. Jensen, G.M. Kirkelund, Sewage sludge ash as resource for phosphorous and material for clay brick manufacturing, Constr. Build. Mater. 249 (2020), https://doi.org/10.1016/j.conbuildmat.2020.118684.
[19] B. Beal, A. Selby, C. Atwater, C. James, C. Viens, C. Almquist, A comparison of thermal and mechanical properties of clay bricks prepared with three different pore-forming additives: Vermiculite, wood ash, and sawdust, env, Prog. Sustain Energy 38 (2019), https://doi.org/10.1002/ep.13150.
[20] H. Insam, B.A. Knapp (Eds.), Recycling of Biomass Ashes, Springer Berlin Heidelberg, Berlin, Heidelberg, 2011, https://doi.org/10.1007/978-3-642-19354-5.
[21] L. Pérez-Villarejo, D. Eliche-Quesada, FcoJ. Iglesias-Godino, C. Martínez-García, FcoA. Corpas-Iglesias, Recycling of ash from biomass incinerator in clay matrix to produce ceramic bricks, J. Environ. Manag. 95 (2012), https://doi.org/10.1016/j.jenvman.2010.10.022.
[22] O. Kizinievič, V. Kizinievič, J. Malaiškienė, Analysis of the effect of paper sludge on the properties, microstructure and frost resistance of clay bricks, Constr. Build. Mater. 169 (2018), https://doi.org/10.1016/j.conbuildmat.2018.03.024.
[23] M. Božič, L. Žibret, D. Kvočka, A.M. Pranjić, B. Gregorc, V. Ducman, Drava river sediment in clay brick production: characterization, properties, and environmental performance, J. Build. Eng. 71 (2023), https://doi.org/10.1016/j.jobe.2023.106470.
[24] I. Kocserha, F. Kristály, Effects of extruder head's geometry on the properties of extruded ceramic products, MSF 659 (2010), https://doi.org/10.4028/www.scientific.net/MSF.659.499.
[25] K.J. Krakowiak, P.B. Lourenço, F.J. Ulm, Multitechnique investigation of extruded clay brick microstructure, J. Am. Ceram. Soc. 94 (2011), https://doi.org/10.1111/j.1551-2916.2011.04484.x.
[26] J. Bourret, N. Tessier-Doyen, R. Guinebretiere, E. Joussein, D.S. Smith, Anisotropy of thermal conductivity and elastic properties of extruded clay-based materials: evolution with thermal treatment, Appl. Clay Sci. 116–117 (2015) 150–157, https://doi.org/10.1016/j.clay.2015.08.006.
[27] T. Buchner, T. Kiefer, L. Zelaya-Lainez, W. Gaggl, T. Konegger, J. Füssl, A multitechnique, quantitative characterization of the pore space of fired bricks made of five clayey raw materials used in European brick industry, Appl. Clay Sci. 200 (2021), https://doi.org/10.1016/j.clay.2020.105884.
[28] T. Buchner, T. Kiefer, M. Königsberger, A. Jäger, J. Füssl, Continuum micromechanics model for fired clay bricks: upscaling of experimentally identified microstructural features to macroscopic elastic stiffness and thermal conductivity, Mater. Des. 212 (2021), https://doi.org/10.1016/j.matdes.2021.110212.
[29] A. Viani, R. Ševčík, M.-S. Appavou, A. Radulescu, Evolution of fine microstructure during firing of extruded clays: a small angle neutron scattering study, Appl. Clay Sci. 166 (2018), https://doi.org/10.1016/j.clay.2018.09.002.
[30] O. Kizinievič, V. Voišnienė, V. Kizinievič, I. Pundienė, Impact of municipal solid waste incineration bottom ash on the properties and frost resistance of clay bricks, J. Mater. Cycles Waste Manag. 24 (2022), https://doi.org/10.1007/s10163-021-01314-4.
[31] M. Dondi, F. Mazzanti, P. Principi, M. Raimondo, G. Zanarini, Thermal conductivity of clay bricks, J. Mater. Civ. Eng. 16 (2004), https://doi.org/10.1061/(ASCE)0899-1561(2004)16:1(8.
[32] T. Buchner, T. Kiefer, W. Gaggl, L. Zelaya-Lainez, J. Füssl, Automated morphometrical characterization of material phases of fired clay bricks based on scanning electron microscopy, energy dispersive X-ray spectroscopy and powder X-ray diffraction, Constr. Build. Mater. 288 (2021), https://doi.org/10.1016/j.conbuildmat.2021.122909.
[33] European Commission, Directive (EU) 2018/850 of the european parliament and of the council of 30 may 2018 amending directive 1999/31/EC on the landfill of waste. https://Eur-Lex.Europa.Eu/Legal-Content/EN/TXT/?uri=celex%3A32018L0850, 2018. (Accessed 12 January 2026).
[34] R. Malviya, R. Chaudhary, Leaching behavior and immobilization of heavy metals in solidified/stabilized products, J. Hazard Mater. 137 (2006), https://doi.org/10.1016/j.jhazmat.2006.01.056.
[35] F.K. Crundwell, The dissolution and leaching of minerals, Hydrometallurgy 139 (2013), https://doi.org/10.1016/j.hydromet.2013.08.003.
[36] S.G. Sahu, N. Chakraborty, P. Sarkar, Coal–biomass co-combustion: an overview, Renew. Sustain. Energy Rev. 39 (2014), https://doi.org/10.1016/j.rser.2014.07.106.
[37] EN 933-1:2012 Test of Geometrical Properties of Aggregates – Part 1: Determination of Particle Size Distribution – Sieving Method, 2012.
[38] K. Pfefferkorn, Ein Beitrag Zur Bestimmung Der Plastizität in Tonen Und Kaolinen, vol. 57, Sprechsaal, 1924.
[39] F.A. Andrade, H.A. Al-Qureshi, D. Hotza, Measuring the plasticity of clays: a review, Appl. Clay Sci. 51 (2011), https://doi.org/10.1016/j.clay.2010.10.028.
[40] ISO 10545-3, Ceramic Tiles - Part 3: Determination of Water Absorption, Apparent Porosity, Apparent Relative Density and Bulk Density, 2018.
[41] EN 12457-2:2002, Characterisation of Waste - Leaching - Compliance Test for Leaching of Granular Waste Materials and Sludges - Part 2: One Stage Batch Test at a Liquid to Solid Ratio of 10 l/kg for Materials with Particle Size Below 4 mm (Without or with Size Reduction), 2002.
[42] S. Tominc, V. Ducman, Methodology for evaluating the CO2 sequestration capacity of waste ashes, Materials 16 (2023), https://doi.org/10.3390/ma16155284.
[43] F. El Fgaier, Z. Lafhaj, F. Brachelet, E. Antczak, C. Chapiseau, Thermal performance of unfired clay bricks used in construction in the north of France: case study, Case Stud. Constr. Mater. 3 (2015), https://doi.org/10.1016/j.cscm.2015.09.001.
[44] E.M. Pérez-Monserrat, L. Crespo-López, G. Cultrone, P. Mozzi, L. Maritan, Clayey materials for traditional bricks production in north-Eastern Italy through a combined compositional study: from firing dynamics to provenance, J. Archaeolog. Sci.: Rep. 54 (2024), https://doi.org/10.1016/j.jasrep.2024.104400.
[45] A. Bubalo, D. Vouk, N. Stirmer, K. Nad, Use of sewage sludge ash in the production of innovative bricks—an example of a circular economy, Sustainability 13 (2021), https://doi.org/10.3390/su13169330.
[46] J.P. Malizia, A. Shakoor, Effect of water content and density on strength and deformation behavior of clay soils, Eng. Geol. 244 (2018), https://doi.org/10.1016/j.enggeo.2018.07.028.
[47] A.S. Babu, T. Leander, Effect of salinity on properties of Clay- A review, in: ICART - 2022 Conference Proceedings, 2022.
[48] A. Adediran, S.M. Kikky, S.K. Adhikary, V. Ducman, P. Perumal, Upcycling municipal solid waste incineration bottom ash in clay-bonded bricks, Ceram. Int. 51 (2025), https://doi.org/10.1016/j.ceramint.2024.12.324.
[49] G. Tarì, J.M.F. Ferreira, A.T. Fonseca, Influence of particle size and particle size distribution on drying-shrinkage behaviour of alumina slip cast bodies, Ceram. Int. 25 (1999), https://doi.org/10.1016/S0272-8842(98)00068-6.
[50] J. Krejsová, R. Kužel, M. Keppert, L. Scheinherrová, A. Vimmrová, New insight into the phase changes of gypsum, Mater. Struct. 57 (2024), https://doi.org/10.1617/s11527-024-02404-z.
[51] M. Broström, S. Enestam, R. Backman, K. Mäkelä, Condensation in the KCl–NaCl system, Fuel Process. Technol. 105 (2013), https://doi.org/10.1016/j.fuproc.2011.08.006.
[52] C. Bories, M.-E. Borredon, E. Vedrenne, G. Vilarem, Development of eco-friendly porous fired clay bricks using pore-forming agents: a review, J. Environ. Manag. 143 (2014), https://doi.org/10.1016/j.jenvman.2014.05.006.

[53] S. Wang, L. Gainey, I.D.R. Mackinnon, C. Allen, Y. Gu, Y. Xi, Thermal behaviors of clay minerals as key components and additives for fired brick properties: a review, J. Build. Eng. 66 (2023), https://doi.org/10.1016/j.jobe.2022.105802.
[54] B. Khuzwayo, Compressive strength and water absorption capacity of clay bricks in South Africa, in: C. Aigbavboa, W. Thwala, D. Aghimien (Eds.), Towards a Sustainable Construction Industry: the Role of Innovation and Digitalisation, CIDB, Springer, Cham, 2022, https://doi.org/10.1007/978-3-031-22434-8_25.
[55] E. Cuadros-Rojas, L. Garcia-Ramond, P. Roca, L. Pelà, Experimental analysis of the compressive behaviour of perforated brick masonry using digital image correlation, Constr. Build. Mater. 431 (2024), https://doi.org/10.1016/j.conbuildmat.2024.136471.
[56] A. Zawada, M. Ulewicz, The influence of addition of fly ash from biomass combustion on selected properties of red building ceramics, Constr. Build. Mater. 448 (2024), https://doi.org/10.1016/j.conbuildmat.2024.138235.
[57] 772-1 SIST EN, Methods of Test for Masonry Units Determination of Compressive Strength, 2015.
[58] W. Cholamjiak, S. Lawanwadeekul, K. Kankam, P. Cholamjiak, N. Jun-On, Classifying compressive strength of clay bricks using aninertial projected forward-backward algorithm, CJM 42 (2026), https://doi.org/10.37193/CJM.2026.02.05.
[59] H. Giesche, Mercury porosimetry: a general (practical) overview, Part. Part. Syst. Char. 23 (2006), https://doi.org/10.1002/ppsc.200601009.
[60] L. Žibret, W. Wisniewski, B. Horvat, M. Božič, B. Gregorc, V. Ducman, Clay rich river sediments calcined into precursors for alkali activated materials, Appl. Clay Sci. 234 (2023), https://doi.org/10.1016/j.clay.2023.106848.
[61] A. Roslin, D. Pokrajac, K. Wu, Y. Zhou, 3D pore system reconstruction using nano-scale 2D SEM images and pore size distribution analysis for intermediate rank coal matrix, Fuel 275 (2020), https://doi.org/10.1016/j.fuel.2020.117934.
[62] A. Popovich, V. Sufiiarov, Metal powder additive manufacturing, in: I.V. Shishkovsky (Ed.), New Trends in 3D Printing, InTech, 2016, https://doi.org/10.5772/63337.
[63] M.L. Elias, G. Cultrone, On the use of sodium chloride and calcined diatomite sludge as additives to improve the engineering properties of bricks made with a clay Earth from Jun (Granada, Spain), Minerals 9 (2019), https://doi.org/10.3390/min9010064.
[64] M. Dondi, G. Guarini, M. Raimondo, Trends in the formation of crystalline and amorphous phases during firing of clay bricks, Tile & Brick Int. 15 (1999).
[65] S. Lawanwadeekul, P. Chindaprasirt, N. Ariyajinno, A. Srisuwan, N. Phonphuak, Acid-resistant clay bricks incorporating bottom ash and waste glass strengthened by mullite suppression and albite formation, Next Mater. 11 (2026), https://doi.org/10.1016/j.nxmate.2026.101610.
[66] N. Phonphuak, S. Lawanwadeekul, P. Chindaprasirt, Fired clay brick containing waste glass and agricultural waste, in: Advances in Sustainable Masonry Bricks and Blocks, Elsevier, 2026, https://doi.org/10.1016/B978-0-443-40389-7.00005-9.
[67] Y. Xing, F. Guo, M. Xu, X. Gui, H. Li, G. Li, Y. Xia, H. Han, Separation of unburned carbon from coal fly ash: a review, Powder Technol. 353 (2019), https://doi.org/10.1016/j.powtec.2019.05.037.
[68] Y.L. Gui, W. Hu, Z.Y. Zhao, X. Zhu, Numerical modelling of a field soil desiccation test using a cohesive fracture model with Voronoi tessellations, Acta Geotech. 13 (2018), https://doi.org/10.1007/s11440-017-0558-9.
[69] C.K. Morley, How successful are analogue models in addressing the influence of pre-existing fabrics on rift structure? J. Struct. Geol. 21 (1999) https://doi.org/10.1016/S0191-8141(99)00075-9.
[70] D. Sergeev, D. Kobertz, M. Müller, Thermodynamics of the NaCl–KCl system, Thermochim. Acta 606 (2015), https://doi.org/10.1016/j.tca.2015.03.003.
[71] Z. Liu, S. Wen, J. Wang, Y. Li, L. Mao, Y. Yang, Z. Liu, Sintering behavior and chlorine volatilization mechanism of Cl-Containing solid waste in clay brick production: implications for tunnel kiln applications, Construct. Mater. 5 (2025), https://doi.org/10.3390/constrmater5020034.
[72] K.S.P. Karunadasa, C.H. Manoratne, H.M.T.G.A. Pitawala, R.M.G. Rajapakse, The composition, unit cell parameters and microstructure of quartz during phase transformation from α to β as examined by in-situ high-temperature X-ray powder diffraction, J. Phys. Chem. Solid. 117 (2018), https://doi.org/10.1016/j.jpcs.2018.02.028.
[73] E. Smadi, A. Chinnici, B. Dally, G.J. Nathan, Effect of heating rate on the kinetics of limestone calcination, Chem. Eng. J. 475 (2023), https://doi.org/10.1016/j.cej.2023.146165.
[74] G. Thalmaier, N. Cobîrzan, A.A. Balog, H. Constantinescu, M. Streza, M. Nasui, B.V. Neamtu, Influence of sawdust particle size on fired clay brick properties, Mater. Construcción 70 (2020), https://doi.org/10.3989/mc.2020.04219.
[75] E. Benavidez, C. Grasselli, N. Quaranta, Densification of ashes from a thermal power plant, Ceram. Int. 29 (2003), https://doi.org/10.1016/S0272-8842(02)00090-1.
[76] RS, Uredba o odpadkih, Ministrstvo Za Okolje in Prostor Vlada Republike Slovenije, 2022. https://pisrs.si/pregledPredpisa?id=URED8482. (Accessed 23 April 2026).
[77] Decree on the Waste Landfill, Council Directive 1999/31/EC of 26 April 1999 on the Landfill of Waste, 1999.
[78] H. Sun, J. Alexander, B. Gove, M. Koch, Mobilization of arsenic, lead, and mercury under conditions of sea water intrusion and road deicing salt application, J. Contam. Hydrol. 180 (2015), https://doi.org/10.1016/j.jconhyd.2015.07.002.
[79] E.C. Rada, M. Schiavon, V. Torretta, A regulatory strategy for the emission control of hexavalent chromium from waste-to-energy plants, J. Clean. Prod.n 278 (2021), https://doi.org/10.1016/j.jclepro.2020.123415.
[80] I. Del Rey, J. Ayuso, A.P. Galvín, J.R. Jiménez, M. López, M.L. García-Garrido, Analysis of chromium and sulphate origins in construction recycled materials based on leaching test results, Waste Manage. (Tucson, Ariz.) 46 (2015), https://doi.org/10.1016/j.wasman.2015.07.051.
[81] M. Coronado, A.M. Segadães, A. Andrés, Using mixture design of experiments to assess the environmental impact of clay-based structural ceramics containing foundry wastes, J. Hazard Mater. 299 (2015), https://doi.org/10.1016/j.jhazmat.2015.07.010.
[82] S. Zhang, Y. Zhang, Z. Qu, Physicochemical property and chromium leaching behavior in different environments of glass ceramics prepared from AOD stainless steel slag, J. Alloys Compd. 805 (2019), https://doi.org/10.1016/j.jallcom.2019.07.065.
[83] C. Liao, Y. Tang, C. Liu, K. Shih, F. Li, Double-barrier mechanism for chromium immobilization: a quantitative study of crystallization and leachability, J. Hazard Mater. 311 (2016), https://doi.org/10.1016/j.jhazmat.2016.03.020.
[84] A.F. Stam, R. Meij, H. Te Winkel, R.J.V. Eijk, F.E. Huggins, G. Brem, Chromium speciation in coal and biomass Co-Combustion products, Environ. Sci. Technol. 45 (2011), https://doi.org/10.1021/es103361g.
[85] D. Shen, Q. Bao, J. Qiu, F. Gu, Z. Wu, M. Wu, W. Guo, Y. Long, Effect of calcium oxide on chromium solidification during the melting of hazardous waste incineration fly ash, J. Environ. Manag. 317 (2022), https://doi.org/10.1016/j.jenvman.2022.115475.
[86] S. Song, A.M. Garbers-Craig, Formation, leachability and encapsulation of hexavalent chromium in the Al_2O_3–CaO–Fe_2O_3–Cr_2O_3 system, J. Eur. Ceram. Soc. 36 (2016), https://doi.org/10.1016/j.jeurceramsoc.2015.12.036.
[87] M. Zhang, C. Yang, M. Zhao, L. Yu, K. Yang, X. Zhu, X. Jiang, Immobilization of Cr(VI) by hydrated Portland cement pastes with and without calcium sulfate, J. Hazard Mater. 342 (2018), https://doi.org/10.1016/j.jhazmat.2017.07.039.
[88] G. Cornelis, T.V. Gerven, C. Vandecasteele, Antimony leaching from MSWI bottom ash: modelling of the effect of pH and carbonation, Waste Manage. (Tucson, Ariz.) 32 (2012), https://doi.org/10.1016/j.wasman.2011.09.018.
[89] G. Cornelis, T. Van Gerven, C. Vandecasteele, Antimony leaching from uncarbonated and carbonated MSWI bottom ash, J. Hazard Mater. 137 (2006), https://doi.org/10.1016/j.jhazmat.2006.04.048.
[90] F.-G. Simon, C. Vogel, U. Kalbe, Antimony and vanadium in incineration bottom ash – leaching behaviour and conclusions for treatment process, Detritus (2021), https://doi.org/10.31025/2611-4135/2021.15115.
[91] Y. Taha, M. Benzaazoua, M. Edahbi, M. Mansori, R. Hakkou, Leaching and geochemical behavior of fired bricks containing coal wastes, J. Environ. Manag. 209 (2018), https://doi.org/10.1016/j.jenvman.2017.12.060.

[92] Q. Tian, B. Guo, S. Nakama, K. Sasaki, Distributions and leaching behaviors of toxic elements in fly ash, ACS Omega 3 (2018), https://doi.org/10.1021/acsomega.8b02096.
[93] G. Mancini, F. Palmeri, A. Luciano, P. Viotti, D. Fino, Partial stabilization of Mo-Containing hazardous wastes using a ferrous sulfate-based additive as a redox agent, Waste Biomass Valor. 11 (2020), https://doi.org/10.1007/s12649-020-01095-1.
[94] A. Keulen, A. Van Zomeren, J.J. Dijkstra, Leaching of monolithic and granular alkali activated slag-fly ash materials, as a function of the mixture design, Waste Manage. (Tucson, Ariz.) 78 (2018), https://doi.org/10.1016/j.wasman.2018.06.019.